Transmissivity and groundwater flow exert a strong influence on drainage density

Elco Luijendijk[1]

[1]Independent researcher, Hanssenstrasse 7, 37073, Göttingen, Germany

Correspondence: Elco Luijendijk (elco.luijendijk@posteo.net)

Abstract. The extent to which groundwater flow affects drainage density and erosion has long been debated, but is still uncertain. Here, I present a new hybrid analytical and numerical model that simulates groundwater flow, overland flow, hillslope erosion and stream incision. The model is used to explore the relation between groundwater flow and the incision and persistence of streams for a set of parameters that represent average humid climate conditions. The results show that transmissivity and groundwater flow exert a strong control on drainage density. High transmissivity results in low drainage density and high incision rates and vice versa, with drainage density varying roughly linearly with transmissivity. The model evolves by a process that is defined here as groundwater capture, whereby streams with a higher rate of incision draw the watertable below neighbouring streams, which subsequently run dry and stop incising. This process is less efficient in models with low transmissivity due to the association of low transmissivity and high watertable gradients. A comparison of different parameters shows that drainage density is the most sensitive to transmissivity, followed by parameters that govern initial slope and ~~stream erosion.~~ baselevel. The results agree with field data that show a negative correlation between transmissivity and drainage density. These results imply that permeability and transmissivity exert a strong control on drainage density, stream incision and landscape evolution ~~and that models~~ . Models of landscape evolution may need to explicitly include groundwater flow.

1 Introduction

Drainage density is a fundamental property of the earth's surface that controls erosion and the transport of water and sediments. Drainage density has been observed to vary with climate, vegetation, relief and soil and rock properties (Tucker et al., 2001b; Luo et al., 2016). Several analytical models have been proposed to explain drainage density and the closely related metric valley spacing (Montgomery and Dietrich, 1992; Howard, 1997; Perron et al., 2008, 2009, 2012). In most of these models streamflow scales with drainage area, and the flow paths of water towards streams and the processes generating streamflow are not specified. However, several studies have suggested that groundwater flow plays an important role in controlling streamflow and drainage density (Carlston, 1963; de Vries, 1994; Dunne, 1990; Twidale, 2004). Direct erosion by groundwater discharge, also termed seepage erosion, and its effect on the initiation and development of channel networks has been explored extensively (Dunne, 1990; Pederson, 2001; Abrams et al., 2009; Brocard et al., 2011). However, apart from direct erosion, groundwater also has an indirect effect on erosion by contributing to streamflow and by controlling the watertable, which in turn affects the

25   storage available in the unsaturated zone and the magnitude and spatial distribution of saturation overland flow (Dunne and Black, 1970; Freeze, 1972; de Vries, 1976).

A number of analyses of river networks have noted a relation between drainage density, lithology and transmissivity (Carlston, 1963; Luo and Stepinski, 2008; Bloomfield et al., 2011). Drainage density has been used infer the transmissivity and permeability of the subsurface (Luo et al., 2010; Luo and Pederson, 2012; Bresciani et al., 2016). A review of drainage density
30   in the conterminous USA found a relation with independent data on subsurface permeability (Luo et al., 2016). These studies imply that a relation exists between permeability, groundwater flow and drainage density. However, to my knowledge a causal mechanism for this relation has not been proposed.

Most numerical landscape models use simplified representations of groundwater flow, and do not simulate the watertable or lateral groundwater flow directly (Tucker et al., 2001a; Bogaart et al., 2003; van der Meij et al., 2018). There are some
35   exceptions, including two case studies of single river catchments (Huang and Niemann, 2006; Barkwith et al., 2015) and a generic model study (Zhang et al., 2016), that concluded that the inclusion of groundwater flow has a strong effect on modelled relief and erosion rates. Recently, a groundwater flow component has been added to the landscape evolution model code Landlab (Litwin et al., 2020). However, to my knowledge there has been no systematic model study to explore the relation between groundwater flow and drainage density.
40   Here, I present a new coupled model of groundwater flow, overland flow and erosion. The model was inspired by the coupled groundwater and streamflow model of de Vries (1994). The model ~~includes~~ simulates lateral groundwater flow, the watertable and its effect on the partitioning of groundwater and overland flow~~and~~. The model also includes erosion processes that follow widely-used equations (Tucker and Hancock, 2010). The model is used to explore the sensitivity of drainage density to parameters that govern groundwater flow, stream flow and erosion. The focus is on humid regions where infiltration-excess
45   overland flow is of minor importance, and where the groundwater system is tightly coupled with the surface water system. The results point to a strong relation between drainage density, groundwater flow and transmissivity. In addition, the results illustrate the process of groundwater capture that explains this relation.

2   Methods

2.1   Model description

50   The model code described here simulates steady-state groundwater flow, transient saturation overland flow, stream incision and hillslope diffusion in a two-dimensional cross-section of the subsurface. These processes are shown schematically in Fig. 1. The model code is named the groundwater flow, overland flow and erosion model, or GOEMod, and was inspired by the conceptual groundwater outcrop erosion model originally presented by de Vries (1976) and subsequently implemented as a set of coupled analytical solutions for groundwater and streamflow (de Vries, 1994). GOEMod is an open source code and is
55   available online on Zenodo (Luijendijk, 2021) and GitHub (https://github.com/ElcoLuijendijk/goemod).

Groundwater flow is approximated as steady-state, with the dark blue line in Fig. 1 showing the average groundwater level. Each precipitation event adds a volume of water on top of the average groundwater level, shown by a light blue area. Saturation

overland flow occurs where the groundwater level is so close to the surface that there is no storage space available in the unsaturated zone. Note that infiltration-excess overland flow is included in the model code, but is not used in this study, because of the focus on humid regions where infiltration excess overland flow is of minor importance (Dunne, 1978; Bogaart et al., 2003). Groundwater flow and saturation overland flow contribute to steady-state and transient streamflow, respectively. Both components of streamflow lead to erosion and incision of the stream. In addition, the areas outside streams erode by hillslope diffusion, which is a simplified representation of processes such as soil creep (Culling, 1960, 1963).

The model starts with a rectangular model domain with a constant slope in one direction. The rectangular model domain contains a single cross-section that is oriented perpendicular to the slope and that is used to solve the groundwater flow, overland flow and the hillslope diffusion equations. The initial topography in the direction of the cross-section is randomly perturbed. The topography evolves over time as a result of stream incision and hillslope diffusion. The model simulates groundwater flow, overland flow and hillslope diffusion in the 2D cross-section. All streams are assumed to run perpendicular to the cross-section and are perfectly straight and parallel. Streamflow and stream incision are calculated by multiplying the water and sediment flux in the 2D cross-section with the contributing area perpendicular to the cross-section. The resulting model is 2.5D in the sense that it simulates water fluxes and incision of a series of perfectly parallel streams that develop along an inclined topography. The workflow and equations for each component of the model are discussed in detail in the following sections.
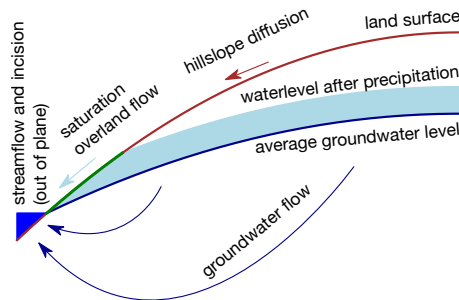
Figure 1. Conceptual model showing the hydrological and erosion process represented in the new model code. The hydrological processes include groundwater flow, overland flow and streamflow. The erosion processes include hillslope diffusion and stream incision.

2.2 Initial topography

The model starts with a random initial topography, which is calculated as using a series of ~~200~~ 400 linear segments with random placement and random perturbation of the elevation at the start and end points of the segments. For the model simulations shown in this study, the average initial elevation is 0 m and the initial relief is 0.5 m.

2.3 Precipitation

Precipitation events are quantified using rainfall intensity statistics for the Netherlands (Beersma et al., 2019), using a precipitation-frequency curve shown in Figure 2. The rainfall-intensity curves follow a generalized extreme value distribution with the parameters given by the following equations (Beersma et al., 2019),:

$$\eta = 1.02 \left(0.239 - 0.0250 \log(D/60.)\right)^{-1/0.512} \tag{1}$$

$$\gamma = 0.478 - 0.0681 \log(D) \tag{2}$$

$$\kappa = 0.118 - 0.266 \log(D) + 0.0586(\log(D)^2) \tag{3}$$

where η is the location parameter, γ is the dispersion parameter and κ is the shape parameter of the distribution and D is the duration of each rainfall event (s). For the model experiments shown in this study a rainfall duration (D) of 3 hours is used. The precipitation depth for a single precipitation event is calculated as:

$$P_d = 1000.0\eta \left(1.0 + \gamma/\kappa(1.0 - T^{-\kappa})\right) \tag{4}$$

where P_d is the rainfall depth per event (m) and T is repetition time (a), which is the reciprocal of precipitation frequency f (a^{-1}). The model simulates overland flow and groundwater recharge for an average year. The total number of precipitation events in a single year is found by adding up a series of precipitation events until the sum of the individual events matches a desired volume for the total annual precipitation (P_t):

$$P_t = \sum_{i=f_1}^{i=f_2} \left(P_d(i)f(i)\right) \tag{5}$$

The precipitation events per year are calculated starting with a frequency (f_1) of 1 a^{-1}. Subsequently higher frequency (and lower magnitude) events are added progressively until the desired amount of total precipitation per year is reached. The precipitation statistics are based on an average humid climate such as the Netherlands, with a total precipitation (P_t) of 0.75 m a^{-1}.

2.4 Partitioning of groundwater and overland flow

The subdivision of precipitation between evapotranspiration, overland flow and groundwater flow in the model is calculated for individual precipitation evens. For each precipitation event groundwater recharge is assumed to equal the available storage in
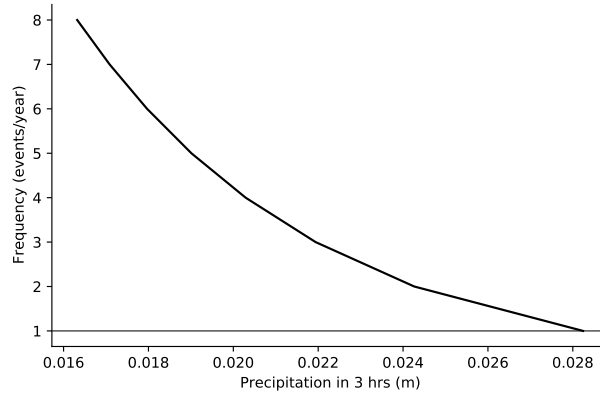
Figure 2. Precipitation frequency curve for the Netherlands, following Beersma et al. (2019) for precipitation events with a duration of three hours. This curve was used to model precipitation, groundwater recharge and overland flow.

100   the unsaturated zone, i.e., all groundwater stored in the unsaturated zone is assumed to eventually percolate to the groundwater table. For each point in the model domain the available storage in the unsaturated zone is calculated using the depth of the watertable and the specific yield of the subsurface as:

$$s = S_y(z - h) \tag{6}$$

where s is storage (m), S_y is specific yield (dimensionless), z is the elevation of the land surface (m) and h is the elevation
105   of the watertable (m). Groundwater recharge for a single precipitation event is calculated as:

$$R_i = \begin{cases} s & \text{if } s < P_d \\ P_d & \text{if } s >= P_d \end{cases} \tag{7}$$

where P_d is precipitation depth per event (m), R_i is groundwater recharge depth per event (m),

The time-averaged potential recharge rate $\overline{R_p}$ (m s^{-1}) is calculated as the sum of the individual recharge events as:

$$\overline{R_p} = \left(\sum_{i=11}^{i=n} (R_i f_i) \right) / \Delta t_r \tag{8}$$

110   where f_i is the frequency of precipitation event i (a^{-1}), and Δt_r is the duration of the reference time period, which is one year (s). The actual recharge rate is calculate by subtracting evapotranspiration:

$$R = \begin{cases} R_p - ET & \text{if } R_p > ET \\ 0 & \text{if } R_p \leq ET \end{cases} \tag{9}$$

where ET is the evapotranspiration rate (m s^{-1}). Note that for simplicity the evapotranspiration rate is assumed to be ~~constant~~ a fixed value and independent of the depth of the watertable.

115   Saturation overland flow is calculated as the amount of precipitation that exceeds the available storage (s) in the unsaturated zone. For each node in the model domain and for each precipitation event the saturation overland flow depth is calculated as:

$$Q_{si} = \begin{cases} P_d - S & \text{if } s < P_d \\ 0 & \text{if } s >= P_d \end{cases} \tag{10}$$

where Q_{si} is the saturation overland flow depth per precipitation event (m).

2.5 ~~Precipitation~~

120   ~~Precipitation events are quantified using rainfall intensity statistics for the Netherlands (Beersma et al., 2019), using a precipitation-frequency curve shown in Figure 2. The rainfall-intensity curves follow a generalized extreme value distribution with the parameters given by the following equations (Beersma et al., 2019),:~~

$$\eta = 1.02\,(0.239 - 0.0250\log(D/60.))^{-1/0.512}$$

$$\gamma = 0.478 - 0.0681\log(D)$$

125    $\kappa = 0.118 - 0.266\log(D) + 0.0586(\log(D)^2)$

     ~~where η is the location parameter, γ is the dispersion parameter and κ is the shape parameter of the distribution and D is the duration of each rainfall event (). For the model experiments shown in this study a rainfall duration () of 3 hours is used. The precipitation depth for a single precipitation event is calculated as:~~

$$P_d = 1000.0\eta\left(1.0 + \gamma/\kappa(1.0 - T^{-\kappa})\right)$$

$$P_t = \sum_{i=f_1}^{i=f_2} \left(P_d(i) f(i) \right)$$

2.5 Groundwater flow

The model is based on the assumption that groundwater flow can be considered to be in steady-state on the timescales of stream and hillslope erosion processes. This was judged to be reasonable because the groundwater flow system reacts much faster than the relatively slow rates of erosion. Given these assumptions, groundwater flow and the position of the watertable can be calculated using analytical solutions of steady-state groundwater flow.

First, the out of plane component of groundwater flow, i.e., groundwater flow parallel to the direction of the nearest stream, is calculated using Darcy's equation and assuming the out of plane hydraulic gradient is equal to the (out-of-plane) slope of the nearest stream:

$$Q_{go} = TS \tag{11}$$

where T is transmissivity ($\mathrm{m^2\,s^{-1}}$), and S is stream slope ($\mathrm{m\,m^{-1}}$). Out of plane groundwater flow can be significant for cases with high transmissivity or stream slope, as shown in Fig. 3.

The remaining in-plane groundwater flow (i.e., towards the nearest stream) is calculated using the value of recharge calculated in equation 8 and subtracting the out-of-plane discharge:

$$R_e = \overline{R}L_u - Q_{go} \tag{12}$$

where R_e is the effective in-plane recharge $\mathrm{m\,s^{-1}}$, and L_u is the length of the upstream contributing area (m).

In-plane groundwater flow is calculated using the Dupuit-Forchheimer equation, which describes depth-integrated, steady-state groundwater flow between two groundwater discharge points (Forchheimer, 1886; Bresciani et al., 2016):
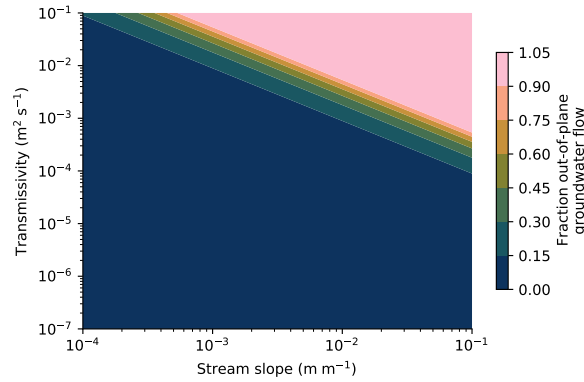
Figure 3. Calculated out-of-plane groundwater flow for a range of values of transmissivity and stream slope, and using the base-case values of contributing area (5 km) and groundwater recharge (0.375 m a^{-1}).

$$\Delta h = \frac{\overline{R_e}}{T} x(L - x) + \Delta H x/L \tag{13}$$

where h is hydraulic head (m), L is the distance between two groundwater discharge points (m), x is the distance to the first discharge point (m) and ΔH is the difference in water level between the two discharge points (m). The term groundwater

160 discharge point represents a point such as a stream or a part of the land surface where the watertable is at the surface and where groundwater seepage takes place. The equation assumes that the lateral differences in hydraulic head (h) are much smaller than the thickness of the aquifer (Bresciani et al., 2016).

For points at the edge of the model domain that are only bound by a discharge point on one side, the equation reduces to:

$$\Delta h = \frac{\overline{R_e}}{T} x(L_b - x) \tag{14}$$

165 Where L_b is the distance between the discharge point and the lateral model boundary (m). The average in-plane groundwater recharge rate $\overline{R_e}$ was calculated as the average effective recharge rate for all the nodes in between two seepage nodes. The seepage nodes represent points where the watertable is at the surface and where groundwater discharge occurs. The position of the seepage nodes is not known in advance, but is calculated using the following iterative procedure:

1. First one seepage node is picked at the lowest elevation in the model domain and the watertable is calculated using
170   equations 13 and 14. In most cases the calculated watertable is still above the land surface in a large part of the model domain after the first iteration.

2. Subsequently a new seepage node is added at the node with the lowest elevation in the part of the model domain where the modelled watertable exceeds the land surface.

3. The watertable is recalculated using this new additional seepage node.

175   4. The last two steps are repeated until the modelled watertable is below or at the land surface (i.e., $h \leq z$) everywhere.

An example of the calculated watertable and seepage locations following the procedure is shown in Fig. 4.
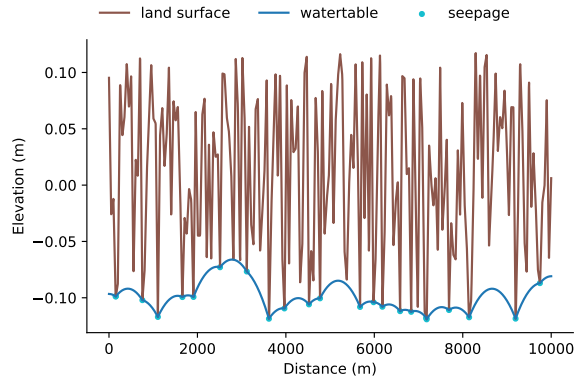
Figure 4. Example of initial topography and calculated watertable and groundwater seepage locations. The watertable and seepage locations were calculated by an iterative solution of eqs. 13 and 14 as explained in section 2.5.

2.6   Stream flow

The water flow in each stream consists of two components, steady baseflow supplied by groundwater discharge, and transient flow that consists of overland flow. The calculation of both components is described in the following two sections:

180   **2.6.1   Baseflow**

The baseflow in each stream node is calculated in two steps. First, streams nodes are found by finding the node with the lowest elevation for each series of neighbouring seepage nodes in the model domain. Note that the term seepage nodes is used here to denote nodes where groundwater discharge occurs. The two-dimensional (in-plane) value of groundwater flow toward each stream node (q_b) is calculated for each stream by finding the nodes contributing groundwater to each stream and by summing

185   the product of the recharge rate at each node R and the width of each node (Δx). The contributing area is found using the taking the watertable h as calculated using equations 13 and 14 and finding the two nodes on either side of each stream where the hydraulic gradient changes direction. The three dimensional (out of plane) value of baseflow was calculated by multiplying in-plane baseflow (q_b) with an upstream length of each stream:

$$Q_b = q_b L_u \tag{15}$$

190   where Q_b is baseflow. An example of the calculate value of baseflow is shown in Fig. 5.
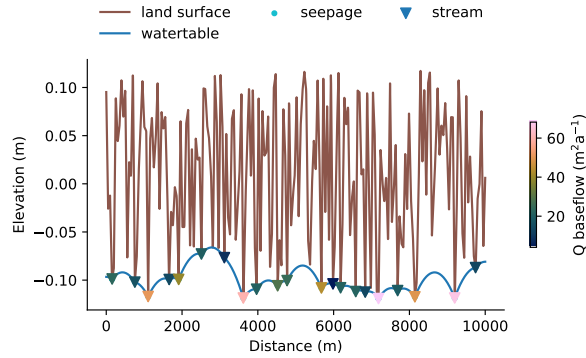
Figure 5. Example of calculated baseflow to streams. The coloured triangles denote the magnitude of the calculated baseflow.

2.6.2 Saturation overland flow

The volume of water that is contributing to overland flow is calculated per precipitation event as:

$$V_0 = \int_{x1}^{x2} Q_{si} dx \tag{16}$$

Where V_0 is the volume of water to be discharged in a stream channel (m^3), x_1 and x_2 are the position of the topographic divide on either side of the channel (m) and Q_{si} is the rate of overland flow for each node as calculated using equation 10. An example of the resulting distribution of precipitation excess and overland flow is shown in Fig. 6.

2.6.3 Waterlevel in streams

The waterlevel in streams as a result of baseflow and overland flow is calculated using the Gauckler-Manning equation for stream discharge. The Gauckler-Manning equation for stream discharge is (Gauckler, 1867; Manning, 1891):

$$v = K_n R^{2/3} S^{1/2} \tag{17}$$

where v is the mean flow velocity in a stream channel (m s^{-1}), K_n is an empirical coefficient (m$^{1/3}$s^{-1}), which is defined as $1/n$ where n is Manning's roughness coefficient (s m$^{-1/3}$), R is hydraulic radius (m) and S is the slope of the water surface, which is taken as equal to the slope of the channel bed (m m^{-1}). With the common assumption that channels are much wider than deep, $R \approx h_c$ and the equation can be simplified to:

$$v = K_n S^{1/2} h_c^{2/3} \tag{18}$$
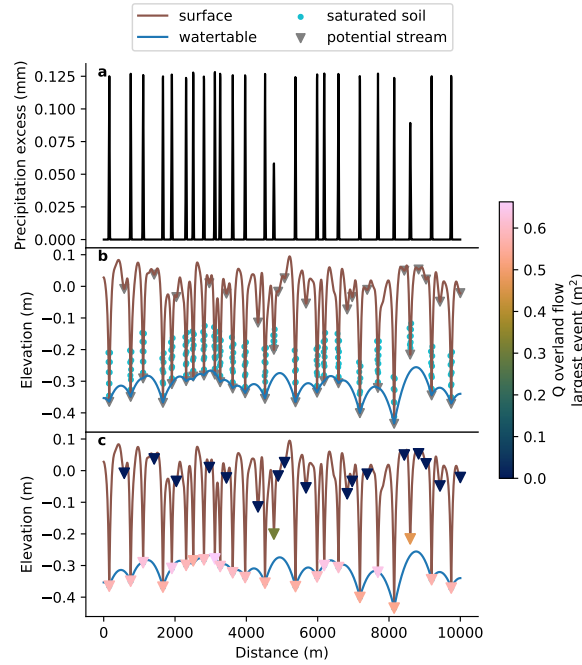
Figure 6. Example of calculated precipitation excess and saturation overland flow in streams. Panel a shows the calculated precipitation excess for each node in the model domain. Panel b shows the location of nodes where the precipitation depth for a single event exceeds the available storage, which results in fully saturated conditions and the generation of saturation overland flow. Panel c shows the calculated saturation overland flow volume for each stream in the model domain. Note that all the potential streams are shown here, including potential streams in depressions that do not generate overland flow because they are located too far above the watertable.

where h_c is the water height in the channel (m). The discharge is equal to the product of the flow velocity and the cross-sectional area. To simplify the equations the cross-section for each stream is assumed to be triangular. The linear in-plane slope of the channel bed (i.e., perpendicular to the flow direction in the channel) is denoted as S_t (m m^{-1}). The cross sectional area A of the channel equals $S_t h^2$. Using this the discharge equation can be written as:

210
$$Q_w = \frac{K_n S^{1/2}}{S_t} h_c^{8/3} \tag{19}$$

where Q_w is the discharge in the channel (m^{3}s^{-1}) and $C_2 = \dfrac{K_n S^{1/2}}{S_t}$. Rewriting this equation yields and expression for the waterlevel in streams as a function of discharge:

$$h_c = \left(\frac{S_t Q_w}{K_n S^{1/2}} \right)^{3/8} \tag{20}$$

2.6.4 Transient stream discharge

215 The discharge generated by overland flow operates on short timescales of hours to days. Modelling this process directly would require short timesteps that would make the model prohibitive computational expensive. Instead here I derive new equations for the total discharge in a stream following a single precipitation event. To keep the solution mathematically tractable the assumption is made that each precipitation event generates a volume of overland flow that is added instantaneously to the stream channel. The volume is subsequently discharged over time.

220 The continuity equation for discharge of a stream channel is given by:

$$\frac{\partial V_w}{\partial t} = -Q_w \tag{21}$$

where V_w is the water volume in the channel (m^3).~~We define the~~ The volume to be discharged is defined as the product of a cross-sectional area that changes over time and a fixed stream length L_u (m):

$$V_w = AL_u \tag{22}$$

225 assuming that the shape of the channel is a triangle and combination with the stream discharge equation (eq. 19) yields:

$$\frac{L_u}{S_t}\frac{\partial h_c^2}{\partial t} = -\frac{K_n S^{1/2}}{S_t} h_c^{8/3} \tag{23}$$

Integration of this equation with boundary condition $h_c = h_0$ at $t = 0$ yields:

$$h_c = \left(h_0^{-2/3} + \frac{K_n S^{1/2}}{3L}t\right)^{-3/2} \tag{24}$$

The initial heigh of the waterlevel in the channel (h_0) is related to the initial volume of water in the channel V_0:

230 $$V_0 = \frac{h_0^2 L_u}{S_t} \tag{25}$$

Adding eq. 25 into eq. 24 and replacing the constants yields an expression for the decrease of waterlevel in a channel over time in response to drainage of an initial volume V_0:

$$h_c = \left(\frac{V_0 S_t}{L_u}^{-1/3} + \frac{K_n S^{1/2}}{3L_u}t\right)^{-3/2} \tag{26}$$

This equation was validated by comparison with a numerical solution of for the waterlevel over time (Fig. 7). The numerical
235 solution was calculated using the discharge equation (eq. 19) to calculate discharge over time. At the first timestep the initial
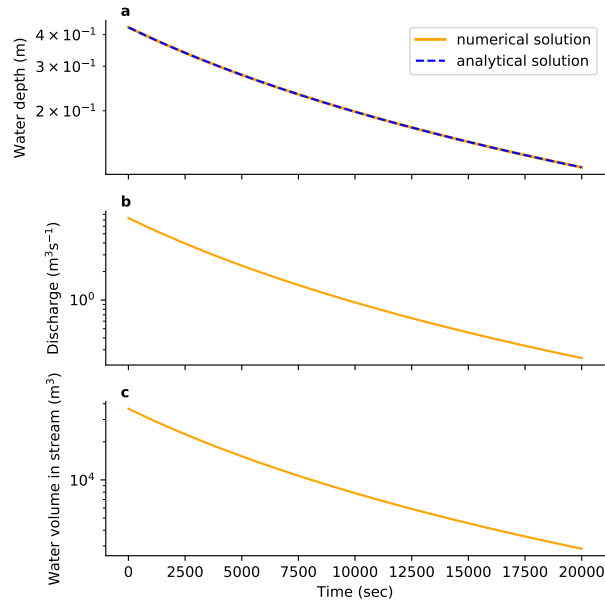
Figure 7. Validation of the equation for the transient discharge of an instantaneously added volume of water in a stream channel (eq. 26) using the numerical solution as described in the text. Panel a shows that the numerical solution and analytical solution overlap perfectly. Panel b and c show the change in water volume and discharge in the channel over time, which were used to calculate the numerical solution in panel a. The solution uses base case parameters listed in Table 1, a precipitation depth of 0.0365 m, which is the theoretical maximum 1-day precipitation depth for a return time of 1 year for the Netherlands, and a contributing area for overland flow with a length of 100 m.

overland flow volume V_0 is added. Subsequently discharge is calculated and subtracted from the initial volume V_0. The heigh of the waterlevel at each timestep was calculated using equation 25. This process is repeated until the waterlevel is less than 1 mm.

2.7 Stream incision

240   The sediment flux in a stream channel at carrying capacity is given by (Tucker and Bras, 1998; Tucker and Hancock, 2010):

$$Q_s = wk_f(Q_w/w)^m S^n \tag{27}$$

where Q_s is the sediment flux $m^3 s^{-1}$, w is channel width (m), k_f is the sediment transport coefficient (~~dimensionless~~$^{4/5}$ m$^{-8/5}$), Q_w is water discharge (m^{-3}s^{-1}), S is channel slope (dimensionless) and m is the discharge exponent (dimensionless) and n is the slope exponent (dimensionless), which were set to values of 1.8 and 2.1, respectively. The erosion by streams is subdivided

245   into two components, the erosion by baseflow driven by groundwater discharge and the additional transient erosion by saturation overland flow during and directly after precipitation events. In addition, incision and stream slope are governed by the

baselevel. The equations for ~~these~~ the calculation of baselevel and the two erosion components are discussed in the following sections.

~~Note that the~~

2.7.1 Baselevel change

The incision of streams results in an adjustment of the stream slope (S). The ~~initial value of~~ stream slope is ~~fixed. After each timestep a new value of stream slope is calculated using the new~~ also dependent on changes in baselevel. The baselevel at the downstream boundary of the model domain is calculated as:

$$z_b = z_{b,0} + Ut \tag{28}$$

where z_b is the ~~base of the stream, and the elevation of the downstream edge~~ downstream model boundary (m), U is the baselevel change rate (m s^{-1}) and t is the total elapsed time since the start of the model run (s). $z_{b,0}$ (m) is the initial baselevel at the start of the model ~~domain, which is assumed not to change over time~~run and is calculated as the product of intial stream slope and distance to the downstream model boundary:

$$~~S~~z_{b,0} = z_0 + S_0 L_d \tag{29}$$

where ~~z_s is the elevation fo the stream in the modelled cross-section (),~~ ~~z_b is~~ z_0 is the average elevation in the ~~elevation of the downstream model boundary (),~~ cross-section at $t=0$ (m), which is 0 m for the model runs shown in this study, S_0 is the initial slope (m m^{-1}) and L_d is the distance to the downstream model boundary (m). ~~The~~

After each timestep a new value of stream slope is calculated using the new elevation of the ~~downstream boundary does not change over time and is the product of the initial slope (S_0) and L_d~~base of the stream and the elevation of the downstream edge of the model domain:

$$S = \frac{z_s - z_b}{L_d} \tag{30}$$

where z_s is the elevation of the stream in the modelled cross-section (m).

2.7.2 Stream incision by baseflow

The sediment flux in the steam channel carried by baseflow is calculated using equation 27 and using the value of baseflow calculated using equation 15 as the value for water discharge Q_w. The incision of the stream is calculated by dividing the sediment flux by the channel width (w). In addition, the erosion is divided over the upstream length of the stream by assuming that erosion increases linearly from zero at the start of the stream to the maximum value at the end of the stream. This yields the following equation for erosion of the stream channel:

$$\frac{\partial z}{\partial t} = (1 - \phi)\frac{Q_s}{w\frac{1}{2}L_u} \tag{31}$$

275   where z is the elevation of the base of the channel (m), t is time (sec), ϕ is porosity (dimensionless). Note that the linear increase of erosion by baseflow along the stream is a simplification that makes the problem more tractable mathematically. In reality the non-linear relation between streamflow and erosion would result in a non-linear increase in erosion along the stream profile.

Channel width was calculated as (Lacey, 1930):

280    $w = k_w Q^\omega \tag{32}$

where k_w and ω are empirical parameters ~~We use~~, which are set to values of $k_w = 3.65$ and $\omega = 0.5$ (van den Berg, 1995).

2.7.3   Stream incision by overland flow

The erosion by streams caused by the discharge of overland flow is calculated by combining the equation for stream discharge due to overland flow over time (eq. 26) with the sediment discharge equation (eq. 27). The combination of these two equations

285   yields:

$$Q_s = k_f S^n \left(\frac{K_n S^{1/2}}{S_t}\right)^m \left(\left(\frac{V_0 S_t}{L_u}\right)^{-1/3} + \frac{K_n S^{1/2}}{3L_u}t\right)^{-4m} \tag{33}$$

Integrating this equation from $t = 0$ to $t = \infty$ yields an expression for the total volume of sediment eroded from the channel after a single precipitation and discharge event:

$$V_s = \frac{a(b + c)^{(-4m+1)}}{4mc + c} \tag{34}$$

290   where V_s is the total volume eroded in a stream by overland flow following a single precipitation event, a, b and c are constants that are defined as:

$$a = k_f S^n \left(\frac{K_n S^{1/2}}{S_t}\right)^m \tag{35}$$

$$b = \left(\frac{V_0 S_t}{L_u}\right)^{-1/3} \tag{36}$$

$$c = \frac{K_n S^{1/2}}{3L_u} \tag{37}$$

The eroded volume results in incision of the stream. Stream incision by overland flow is calculated by distributing the eroded volume (V_s) evenly over the width of the stream channel (w). In addition, erosion by overland flow is assumed to increase linearly from the start of the channel to the position of the modelled cross-section. This is a similar simplifcation as the linear increase of erosion by baseflow discussed in the previous section, and was likewise also used to keep the problem mathematically tractable. This yields the following expression for the incision of the stream due to overland flow:

$$\Delta z_s = \frac{V_s}{(w \frac{1}{2} L_u)} \tag{38}$$

where Δz_s is stream incision following a single precipitation event (m).

2.8 Hillslope diffusion

Erosion of the parts of the model domain outside of the streams follows the hillslope diffusion equation (Culling, 1960):

$$\frac{\partial z}{\partial t} = \frac{\partial \left(K_d \frac{\partial z}{\partial x} \right)}{\partial x} \tag{39}$$

Where K_d is the hillslope diffusion coefficient ($m^2\,s^{-1}$). This equation was solved numerically using a standard implicit finite difference approach using a matrix solver implemented in the Python module Numpy (Harris et al., 2020).

2.9 Iterative solution

The solution of the equations for groundwater flow, overland flow, streamflow and erosion follow an iterative scheme that is detailed in Fig. 8. After setting up an initial topography, the initial watertable is calculated using the procedure described in section 2.5, with recharge taken as the difference between the total precipitation (P_t), overland flow and evapotranspiration (ET). Subsequently the model calculates baseflow, stream incision due to baseflow and overland flow, and topography change due to hillslope diffusion. Overland flow and recharge are calculated at an event basis. Recharge is summed over a year to yield an average recharge rate. Overland flow and erosion are calculated on an event basis, and are then summed over a year to yield an average overland flow erosion rate. The procedure is repeated at each timestep. The initial timestep size is 1 year. The timestep size is was adjusted so that the maximum elevation change per timestep was 0.5% of the total relief with a minimum of 0.01 m. These conditions were found by trail and error to ensure numerically stable and computationally efficient model runs for the range of parameter values and runs reported in this study.

2.10 Base case parameter values

The base case parameter values follow ~~Bogaart et al. (2003)~~ de Vries (1994) and Bogaart et al. (2003), who modelled stream network and landscape evolution ~~for north-western Europe~~ of the southern Netherlands under alternating glacial and interglacial conditions. Here the parameters that represent present-day (interglacial) conditions are used. The base case parameters are listed
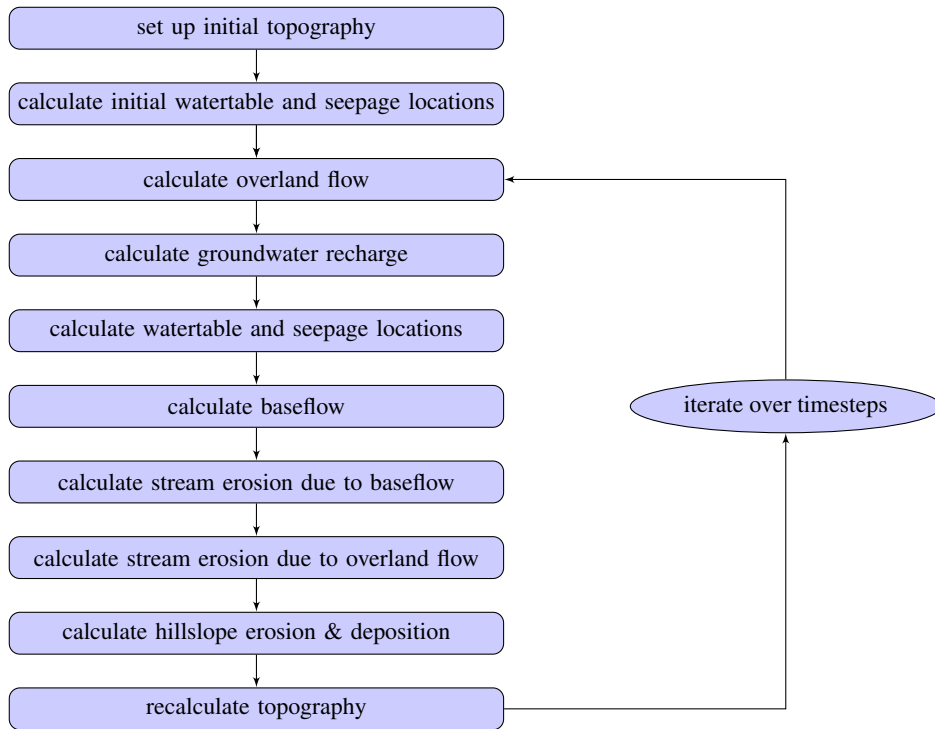
Figure 8. Flowchart for the iterative solution of the groundwater flow, overland flow and erosion equations

in table 1. In contrast to the relatively high value for porosity of 0.4 used by Bogaart et al. (2003) here a value of 0.2 is used that more closely follows values observed in areas covered by fluvial and aeolian sediments in the southern Netherlands (de Vries, 1994). The base case value for transmissivity is ~~1×10^{-3}~~ 1×10^{-2} m^{2}s^{-1}, which is ~~lower than~~ based on values of 0.012 to

325 0.03 m^{2}s^{-1} reported by de Vries (1994). The ~~relatively low value of transmissivity was chosen because higher values led to a very low drainage densities, which made them less suitable as a starting point for sensitivity analyses. For~~ initial slope a value of ~~5×10^{-3} was chosen, which is higher than~~ of 5×10^{-4} m m^{-1} is equal to the average stream gradient in the ~~Netherlands~~ southern Netherlands.

The value of the sediment transport coefficient reported by Bogaart et al. (2003) was based on the theoretical Einstein-Brown

330 equation. Here, the value of this parameter is based on an analysis of alluvial sediment discharge data by Brownlie (1981) as reported by Lammers and Bledsoe (2018). Following the sediment discharge equation (eq. 27) the sediment transport coefficient (k_f) can be expressed as:

$$k_f = \frac{q_s}{q_w^m S^n} \tag{40}$$

The compilation of total sediment discharge from flume experiments and field observations by Brownlie (1981) as reported

335 by Lammers and Bledsoe (2018) contains $n = 1463$ datapoints for which sediment discharge (q_s), water discharge (q_w) and
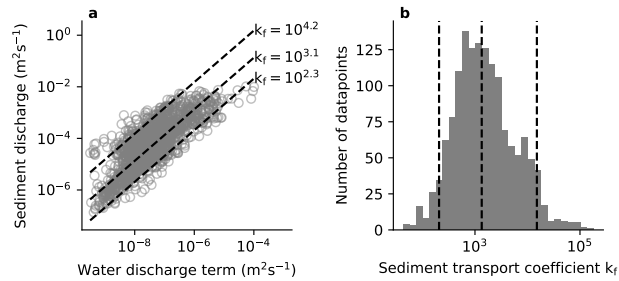
Figure 9. Comparison of measured sediment discharge and the water discharge term $q_w^m S^n$ in the sediment discharge equations (eq. 27 and 40) (panel a) and the calculated variation of the sediment transport coefficient (panel b) in a compilation of 1463 sediment discharge data from flume experiments and field observations by Brownlie (1981) as reported by Lammers and Bledsoe (2018). The lines in panel a and b denote the 0.05, 0.5 and 0.95 quantiles of the distribution of k_f as calculated using equation 40.

stream slope (S) are known. Following Bogaart et al. (2003) the coeficients n and m are set to values of ~~5×10^{-4}. Lower values resulted in models where channel initiation was so slow that~~ 1.8 and 2.1 respectively. Inserting these values into equation 40 allows k_f to be calculated for each of the 1463 datapoints. The calculated distribution of k_f using equation 40 is shown in Fig. 9. Comparison of the measured sediment discharge values and the denominator ($q_w^m S^n$) in equation 40 shows that there 340 is a reasonable correlation of the term $q_w^m S^n$ with the sediment discharge rate. When using the median value of $k_f = 10^{3.1}$ to predict sediment discharge, the coefficient of determination for log-transformed values of sediment discharge equals 0.62. The median value of $k_f = 10^{3.1}$ was used as the ~~modelled drainage density reflected the initial random topography, as will be further discussed in section 4.1.~~ base-case parameter value for the model experiments shown in this study. Note that more complex sediment transport equations that take into account sediment grain size and transport thresholds yield a closer fit to 345 the data (Lammers and Bledsoe, 2018). However, these equations were not implemented in this study to keep the calculation of sediment discharge for individual discharge events (equation 34) mathematically tractable.

2.11 Model sensitivity analyses

To explore the role of groundwater flow in erosion a series of model experiments were conducted with different values for transmissivity and specific yield. To compare the effects of changes in groundwater flow with climate and erosion parameters, 350 an additional set of experiments was conducted with different values for total precipitation (P_t), hillslope diffusion coefficient (K_d)~~and slope exponent (~~, sediment transport coefficient (k_f) and baselevel change (U). These values are listed in table 2.

The range of variation of the hillslope diffusion coefficient was based on Richardson et al. (2019). There are no large compilation of transmissivity available. Models and data of the permeability of unconsolidated sediments (Gleeson et al., 2011; Luijendijk and Gleeson, 2015) and ~~an~~ a hydrologically active layer of approximately 100 m (Gleeson et al., 2016; Jasechko 355 et al., 2017) suggests a variation of approximately 10^{-7} to 10^{-1} m^2 s^{-1}. Here a smaller range of values is evaluated, 10^{-4} m to 10^{-1} m, because ~~lower values~~ for the relatively low-relief landscape that was studied, lower values of transmissivity result

Table 1. Base case parameter values

parameter group	parameter name	symbol	value	
Model geometry	length	L	~~10000~~ 20000 m	
	upstream length	L_u	~~5000~~ 10000 m	
	downstream length	L_d	~~5000~~ 10000 m	
	grid cell size	Δx	5 m	
Relief	initial relief		0.5 m	
Precipitation and ET	precipitation event duration	D	1.0 day	
	annual precipitation	P	0.75 m a^{-1}	F
	potential ET	ET	0.375 m a^{-1}	F
Stream flow	channel roughness factor	K_n	25	
	initial channel slope	S_0	~~5×10^{-3}~~ 4×10^{-4}	
	perpendicular channel slope	S_t	~~0.05~~ 0.002	
	channel width coefficient 1	k_w	3.65	v
	channel width coefficient 2	ω	0.5	v
Groundwater flow	specific yield	S_y	0.2	
	transmissivity	T	~~1×10^{-3}~~ 1×10^{-2} m^2 s^{-1}	
Erosion	base level change	U	-10^{-5} ma^{-1}	B
	sediment transport coefficient	k_f	~~0.32~~ $10^{3.1}$	~~Tucker and Bras (1998)~~ Brownlie (1981); Lammers a
	discharge exponent	m	1.8	F
	slope exponent	n	2.1	F
	hillslope diffusion coefficient	K_d	0.01 a^{-1}	F
	porosity	ϕ	0.2	

in drainage densities that are fully controlled by the initial random topography. The values of specific yield are based on values reported for mixed sediments (Revil, 2002; Gleeson et al., 2014; El-husseiny, 2020). The ~~variation of the slope exponent was based on a global compilation by Harel et al. (2016).~~ minimum and maximum values for sediment transport coefficient were

360 equal to the 0.05 and 0.95 quantiles of the calculated distribution of k_f shown in Fig. 9.

2.12 Additional model experiments

In addition to the model sensitivity analysis a second set of model experiments was conducted to explore the persistence of drainage density over longer timescales. These model experiments used the modelled incised topography of the base-case model run after 10,000 years as a starting point, and subsequently added another 50,000 years to the simulation, but with

365 different parameter values that follow the sensitivity analysis reported in the previous section and Table 2. These different

Table 2. Parameter value range in model sensitivity analyses

parameter name	symbol	value, minimum	value, maximum	number of steps
precipitation	P	0.5 m a^{-1}	~~1.0~~ 1.5 m a^{-1}	10
transmissivity	T	1×10^{-5} m	1×10^{-1} m	10
specific yield	S_y	0.15	0.5	10
hillslope diffusion coefficient	K_d	4×10^{-5} m^2 a^{-1}	4×10^{-2} m^2 a^{-1}	10
~~stream slope~~ sediment transport coefficient	k_f	~~1×10^{-4}~~ $10^{2.3}$	~~0.025~~ $10^{4.2}$	10
~~slope exponent~~ baselevel change	U	~~1.0~~ 10^{-5} m a^{-1}	~~2.6~~ 10^{-3} m a^{-1}	10

parameter values resulted in model simulations where the system was out of balance with the incised topography. The degree to which these runs resulted in an adjustment of the stream network and drainage density after a runtime of 10,000 and 50,000 years was recorded and used to quantify the persistence of stream networks.

3 Results

3.1 Groundwater capture

Figure 10 shows the result of an example model run using the base case parameters values as shown in Table 1. The figure shows the evolution of the land surface from an initial randomly generated surface over a timespan of ~~100~~10,000 years. The system starts out with a very high drainage density, with ~~65 streams~~ 114 streams in a model domain that is 20 km long. Subsequently the model evolves rapidly towards a system dominated by fewer streams over time, with the final number of ~~13~~ 12 active streams after a runtime of ~~100~~10,000 years.

The decrease in number of streams is caused by a process that is ~~referred to~~ defined here as groundwater capture, by which faster eroding streams draw the watertable below neighbouring streams and reduce the baseflow and saturation overland flow of these streams until they fall dry. The process of groundwater catchment capture is illustrated in more detail in Figure 11, which shows the land surface, watertable and stream fluxes for three timeslices before, during and after a groundwater catchment capture event. After ~~73~~ 2251 kyr (Fig. 11a) there are still ~~15~~ 13 streams that are active. However, the ~~second stream from the left~~ last stream on the right hand side has smaller catchment area and a lower baseflow, and therefore incises slower than its two neighbouring streams. After ~~79 kyr~~ 2457 yr (Fig. 11b) the neighbouring streams have incised further and have drawn the watertable below the base of the stream. The second stream does generate overland flow, but has ceased to generate baseflow. At ~~86 kyr~~ 2707 yr the watertable has been drawn down further and the watertable is too deep for the second stream to generate saturation overland flow, i.e., all the precipitation that falls near the stream can be accommodated in the unsaturated zone above the watertable. As a results the stream has become inactive. The stream channel has partly been filled by hillslope diffusion, because the sediment flux caused by hillslope diffusion is no longer compensated by the removal of sediment by streamflow.

The evolution of the stream network over time is ~~summarized~~ summarised in Figure 12. Initially each small depression is potentially an active stream channel, which results in a large number of active streams. However, as the incision of streams increases, the number of active streams drops rapidly in the first ~~15 kyr~~100 yr, followed by a slower reduction in the number of active streams ~~for the remainder of the model run~~. The last stream capture event at 2457 yr is shown in Fig. 11. After this event the drainage system remains in a steady-state. ~~The continuing~~

The initially high rate of groundwater capture is slowed down over time by the negative feedback imposed by the baselevel at the downstream (out of plane) end of the model domain. The stream slope is lower for streams that have incised deeper, which limits their incision power. The negative feedback on incision results in the establishment of a steady-state drainage network after 2500 years. For the base-case model run shown in Fig. 10, the baselevel is located at an elevation of -4 m, at a downstream distance of 10,000 m.

The incision and the reduction of active streams by groundwater capture also means that the area susceptible to saturation overland flow decreases over time, because saturation overland flow takes place near active stream channels where the watertable is located close to the surface. Apart from a short phase at the start of the model run streamflow and stream erosion are predominantly generated by groundwater flow, which is named baseflow once it enters the stream channel (Fig. 12b, c).
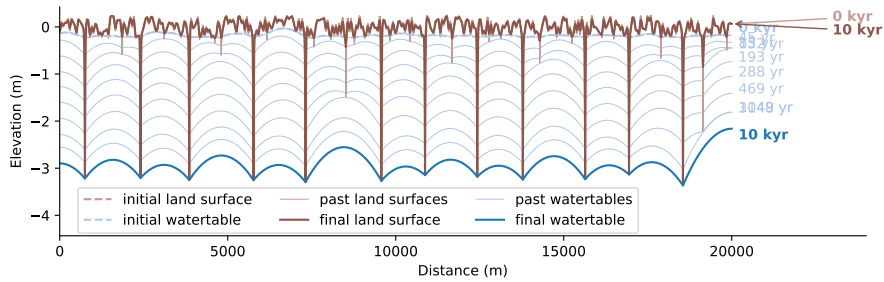
Figure 10. Modelled change in land surface and watertable over ~~100~~10,000 years for the base case model run. The results show the evolution from a random topography ~~to~~ with a ~~system~~ high number of streams to an incised topography with ~~13~~ 12 active streams. The past positions of the land surface and watertable show ~~that~~ the decrease of the number of ~~active~~ streams ~~decreased~~ over time. ~~The time between each past watertable position that is shown is 10,000 years.~~
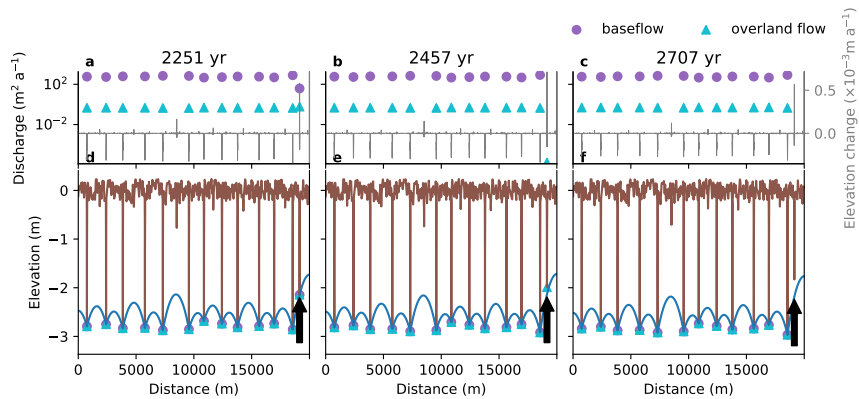
Figure 11. Illustration of groundwater capture in the base case model run. Panel a, b, c show modelled streamflow generated by baseflow and overland flow, and the change in elevation caused by hillslope diffusion and stream erosion for three timeslices before, during and after a capture event, respectively. Panels d, e and f show the modelled position of the land surface and the watertable during these three timeslices. The arrow points to the stream that loses its connection to the groundwater table.
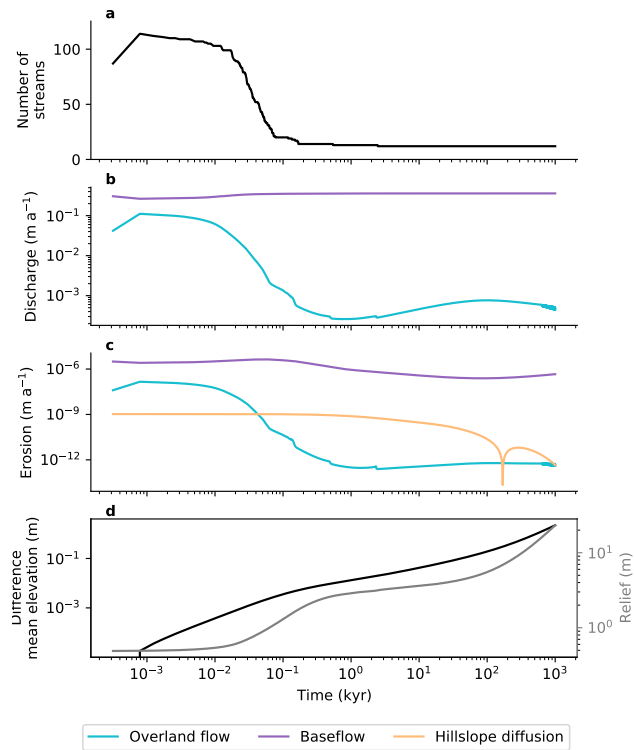
Figure 12. Changes in drainage density (panels a), water discharge (panel b), sediment flux (panels c) elevation and relief (panels d) over ~~time~~ a timespan of 1 million years for the base-case model run. The results show a decrease of active stream channels and a decrease in saturation-excess overland flow over time as streams incise and the watertable is drawn deeper below the land surface.

3.2 Sensitivity of drainage density to transmissivity

Groundwater capture is dependent on the transmissivity of the subsurface. This is illustrated by three model runs with different values of transmissivity (Fig. 13). The model run with the lowest transmissivity shows the ~~higher~~ highest drainage density (Fig. 13a) and ~~a~~ the model run with a ~~high~~ highest value of transmissivity shows ~~a low~~ the lowest value of drainage density (~~(~~Fig. 13c). The reason is that a low transmissivity results in higher watertable gradients, which makes it much more difficult for streams to draw the watertable below neighbouring streams and to capture their groundwater discharge. In contrast, high transmissivity results in a relatively flat watertable, which means that small differences in incision can already lead to a watertable that is drawn below the base of streams. There is a small positive correlation between transmissivity and stream incision rate. The lower number of streams at high values of transmissivity means that these streams receive more water and therefore have a higher erosion power. ~~However, at high transmissivity the groundwater flow direction also changes and the proportion of out-of-plane groundwater flow increases (Fig. 3) . This results in a lower in-plane groundwater flow toward streams and lower incision rates at high transmissivities. These two mechanisms compete with each other. At transmissivities exceeding $10^{-2.0}$ the increase in out-of-plane groundwater flow becomes dominant and results in a decrease in incision rate (Fig. 14).~~ This effect is limited by the negative feedback on stream incision that results from a decrease in stream slope between the modelled cross-section and the baselevel at the downstream (out-of-plane) end of the model domain. For streams with a higher rate of incision, the slope is reduced and their erosional power is reduced.
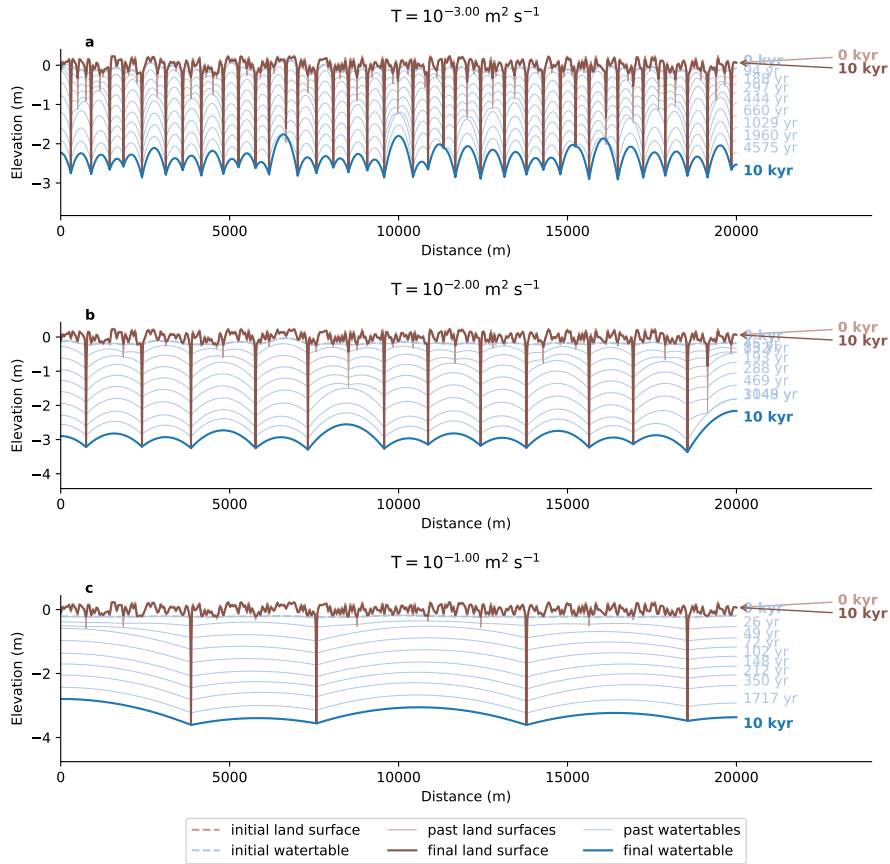
Figure 13. Modelled change in land surface and watertable over time for three model experiments with low (~~$T = 10^{-4}$~~ $T = 10^{-3}$ m^{2}s^{-1}, panel a), moderate (~~$T = 10^{-3}$~~ $T = 10^{-2}$ m^{2}s^{-1}, panel b) and high (~~$T = 10^{-2}$~~ $T = 10^{-1}$ m^{2}s^{-1}, panel c) transmissivity. The results show a negative correlation between drainage density and transmissivity and a positive correlation between transmissivity and stream incision over the model runtime of ~~100~~10,000 years.

3.3 Sensitivity of drainage density to hydrological and erosion parameters

Comparison of drainage density and incision to a number of parameters that govern erosion and streamflow show that drainage density is the most sensitive to transmissivity ~~, followed by stream slope and slope exponent~~ and initial slope (Fig. 14). Drainage density is ~~positively correlated with slope exponent, hillslope diffusion coefficient and precipitation,~~ also affected by precipitation and baselevel change, and ~~is negatively correlated with transmissivity and initial stream slope~~ largely insensitive to specific yield, sediment transport coefficient and hillslope diffusion coefficient.

The strong negative correlation of drainage density and initial downstream slope is illustrated in Fig. 15 and can be explained by ~~two~~ three effects. First, higher stream slope means that individual streams have a higher incision power, which means that it is easier to draw the watertable below adjacent streams and capture their groundwater discharge. Second, a higher stream slope means a lower baselevel at the downstream end of the model domain, which means that streams can incise deeper and capture more adjacent streams before the negative feedback kicks in that is associated with deep incision and a reduction in stream slope. Third, a higher initial downstream slope means that more of the total groundwater recharge is directed downstream in the out-of-plane direction, and there is less in-plane groundwater flow (Fig 3). This results in flatter watertables and an increase in groundwater capture. ~~The slope exponent results in similar magnitude of changes in drainage density and stream incision~~

Precipitation shows a complex relation with drainage density (Fig. 14), with ~~low slope exponents resulting in high incision rates and few streams, and vice versa.~~

~~The effect of changes in hillslope diffusion rate on the development of streams is illustrated in Fig. 16. As many previous studies have highlighted (Tucker and Bras, 1998; Perron et al., 2008), hillslope diffusion competes with stream incision. Hillslope erosion provides a negative feedback on stream incision. Streams incision increases the topographic gradient, which increases hillslope erosion and sediment delivery to the stream, which slows down incision. In models with high hillslope diffusion rates this mechanism is much more dominant, and results in much smaller differences in incision rates between different streams. This results in less groundwater capture and more streams that survive. In contrast, in models with low hillslope diffusion coefficients, differences in incision rates due to differences in groundwater catchment size are not compensated by increases in sediment delivery to streams~~

~~Interestingly, precipitation~~ and specific yield have a limited effect on drainage density (Fig. 14). a positive correlation between drainage density and precipitation at moderate to high values of precipitation, but very high drainage density and low incision rates at low values of precipitation. Precipitation affects groundwater recharge. Given that groundwater flow depends on the ratio of recharge over transmissivity (see eq. 13), ~~in principle~~ recharge has an effect of equal magnitude as transmissivity, but opposite sign. ~~However, the variability of transmissivity of the subsurface is several orders of magnitude, whereas the variability of groundwater recharge is much lower, approximately one order of magnitude in humid regions (Moeck et al., 2020). This results in an overall much more important effect of transmissivity on drainage density~~ I.e., high precipitation and recharge result in high drainage densities and vice-versa. However, at low values precipitation this trend is reversed, because all recharge contributes to out-of-plane groundwater flow and the in-plane groundwater flow, baseflow and overland flow rates are too low for the streams to incise. This means that the initially high number of streams does not decrease over time.

Specific yield only has a subtle effect on stream incision. Lower values of specific yield increase the volume of saturation overland flow and make it more difficult for streams to run completely dry, even if they are disconnected from the watertable. However, given the subordinate importance of overland flow in generating streamflow and erosion in these model experiments, this effect is very modest and does not change the modelled drainage density or incision rate after a model runtime of ~~100~~10,000 years (Fig. 14).

The sediment transport coefficient exerts a strong control on the rate of incision and controls how fast the drainage network reaches a steady-state. High sediment transport coefficients result in high rates of incision and a relatively fast adjustment of the stream network. However, ultimately the rate of incision is limited by the baselevel at the downstream end of the model domain as explained previously, and as a result the sediment transport coefficient only has a minor effect on the modelled drainage density (Fig. 14).

The effect of changes in hillslope diffusion rate on the development of streams is illustrated in Fig. 16. Although hillslope diffusion may be important in determining drainage density in landscapes with higher relief (Tucker and Bras, 1998; Perron et al., 2008), in this case the incision power of streams is high enough to outpace sediment delivery by hillslope diffusion, and the sensitivity analysis shows no effect of hillslope diffusion on drainage density (Fig. 14). The results do show an effect of the lateral slope of stream valleys and on the rate of infilling of abandoned stream channels (Fig. 16).
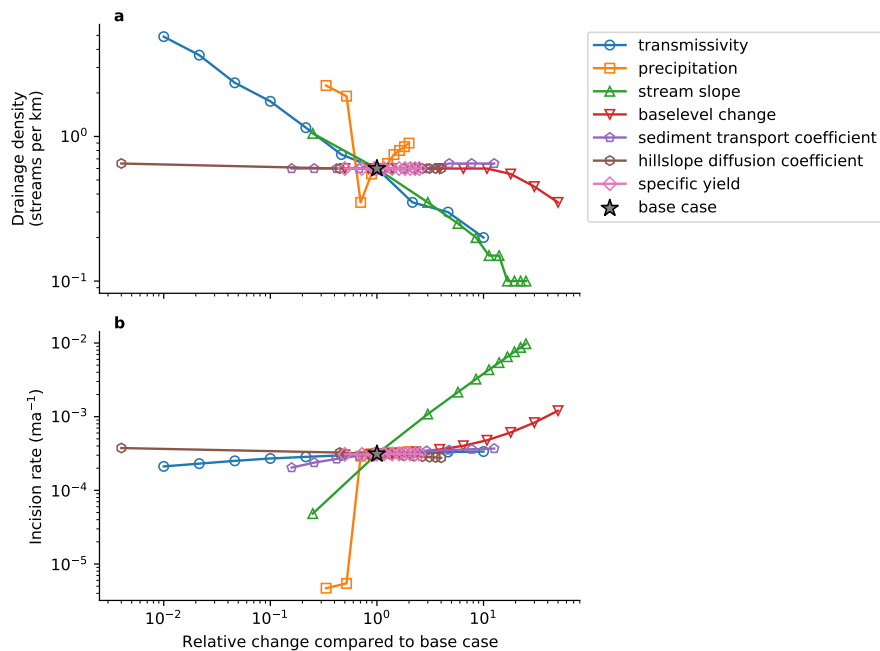
Figure 14. Sensitivity of drainage density and stream incision to hydrological and erosion parameters. The incision rate denotes the incision rate of the stream with the lowest elevation at the end of each model run. Note that the range of parameter values reflects their variability in humid and subhumid settings as explained in the text.
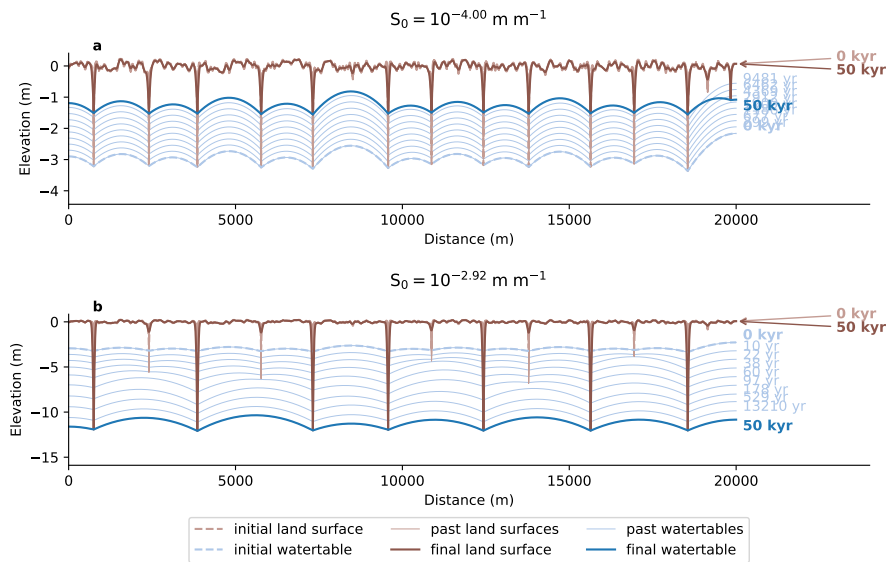
Figure 15. Sensitivity of drainage density and stream incision to initial slope, showing the effects of the lowest (panel a) and highest (panel b) slope that was included in the model sensitivity analysis. Low slopes result in a very low incision power, whereas high slopes provide much more incision power that allows the system to evolve to a situation with fewer active streams. In addition, for low slopes incision is limited by a relatively high baselevel at the downstream end of the model domain, whereas for high slopes the baselevel is much lower. The baselevel for the model experiments shown in panel a and b is located at -2 m and -13 m, respectively.
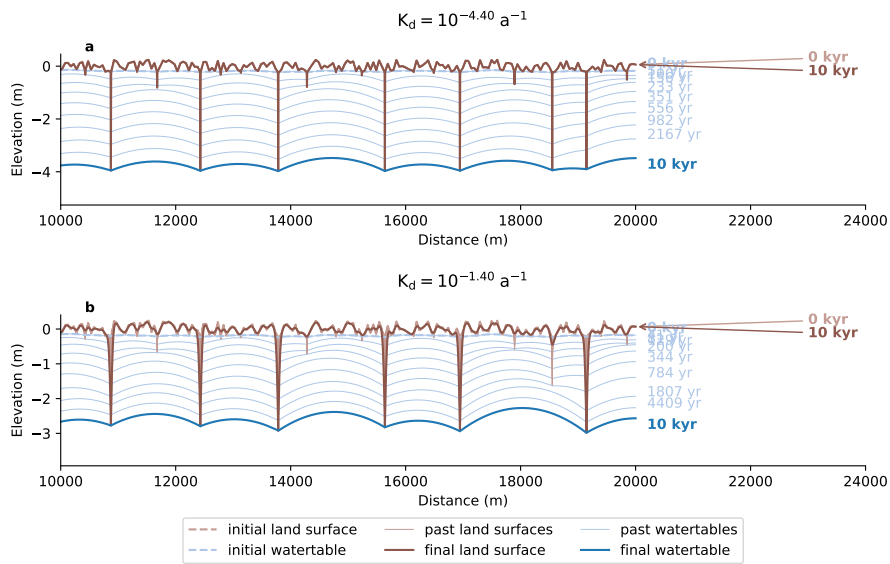
Figure 16. Sensitivity of drainage density and stream incision to hillslope diffusion rate, showing the effects of the lowest (panel a) and highest (panel b) hillslope diffusion rates found in a compilation by Richardson et al. (2019). Note that only half of the model domain is shown here to better visualise the effects of hillslope diffusion on valley slope and infill of inactive stream channels.

3.4 The persistence of stream networks

The model runs shown up to this point all started with a flat topography with a random perturbation of ± 0.5 m. However, in most natural systems the current drainage network started out on an older network that was for instance adjusted to glacial conditions during the Pleistocene. The effect of an existing incised topography on the modelled adjustment of stream networks is shown in Figures 17 and 18.

Figures 17 shows the change in stream network following a change in slope and baselevel. The results indicate that preexisting incised topography delays the evolution of stream networks to higher drainage densities, whereas an evolution to lower drainage density proceeds more rapidly. A decrease in slope S_0 from the base case value of 4×10^{-4} m m^{-1} to 1×10^{-4} m m^{-1} leads to a decrease in incision over time. However, the effect on drainage density is limited. The drainage density is increased only after approximately 9000 years when the decrease in incision has progressed far enough that the watertable reconnects with a previously abandoned stream channel on the right-hand side of the model domain (Figure 17a). This demonstrates that the stream network shows a degree of delay in adjustment to new conditions that depends on the depth of the watertable and the ability of the watertable to reconnect to abandoned stream channels or depressions in the landscape. Conversely, an increase in slope leads to an increase in incision that allows the process of drainage capture to proceed (Figure 17b). Differences in catchment size lead to differences in incision rates and the capture of the groundwater discharge of several small streams by neighbouring streams. This results in a reduction of active streams over time from 12 to 7.

The asymmetry in the response of the drainage network to parameter changes is also shown in the model sensitivity analyses presented in Figure 18. Compared to model runs that start with a flat topography (Figure 18a), the model runs that started with an incised topography (Figure 18b, Figure 18c) show a comparable response when the parameter change leads to a reduction in drainage density. However, an increase in drainage density is much harder to accomplish, because an increase in drainage density is only possible when the watertable is close to the surface. For systems where incision has progressed far enough for the watertable to be well below the surface this requires large changes in precipitation, or a large decrease of incision. The adjustment of incision also means that the time that has elapsed since a parameter change is important for drainage density. The delay in adjustment affects models after a runtime of 10,000 years (Figure 18b), but is much less important for model runs that last 50,000 years (18c). The exception is formed by changes in transmissivity, for which the effect is strong enough to generate a fast response in both directions, i.e. for both an increase and decrease in drainage density. However, abrupt changes in transmissivity are probably somewhat unlikely in reality. They could occur for areas with a gain or loss of permafrost (Bogaart et al., 2003), or in the case of the erosion of a confining layer that shields a more permeable layer.
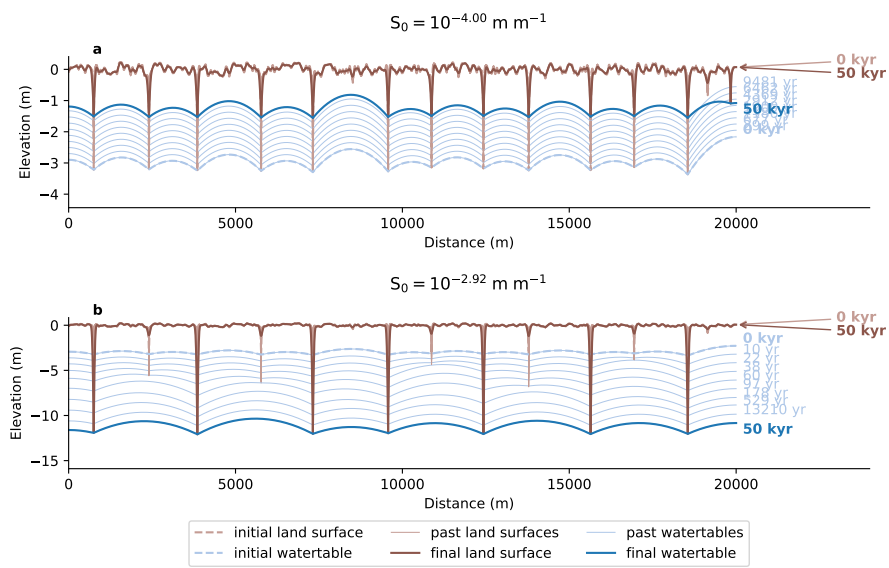
Figure 17. Modelled adjustement of a stream incision for a decrease (panel a) and increase (panel b) in slope. The results show that a decrease in slope and the corresponding increase in baselevel downstream leads to a reduction of stream incision (panel b) and vice-versa (panel b).
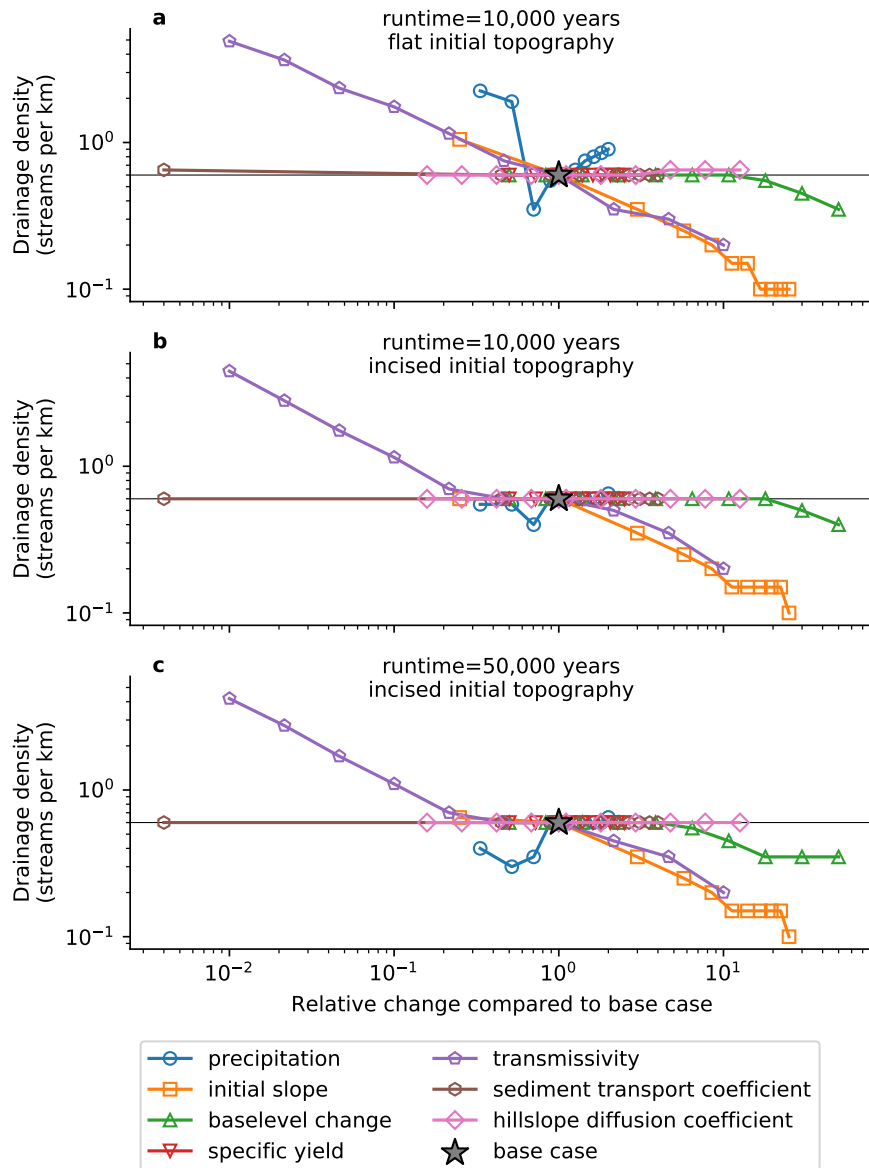
Figure 18. Sensitivity of drainage density to climate, hydrology and transmissivity parameters for using different initial topographies and runtimes. Panel a shows the sensitivity using a flat initial topography with a perturbation of 0.5 m. Panels b and c use an incised initial topography, which is equal to the final topography of the base case model run after a runtime of 10,000 years. For panel b the simulation is run for 10,000 years and for panel c the runtime is 50,000 years. The results show that using an incised initial topography reduced the sensitivity of drainage density to transmissivity and other parameters.

4 Discussion

4.1 Limitations of the model code

The model code presented here was intentionally kept as simple as possible to keep the ~~solution~~ solutions mathematically tractable and the computational effort manageable. The main limitations are that the model is 2.5D and only represents a system with perfectly parallel and straight streams, groundwater flow is steady-state and the contribution of transient groundwater discharge or subsurface stormflow to streamflow is neglected, and the treatment of erosion by overland flow is highly simplified, with an instant addition of all overland flow to the nearest active stream channel, and a highly simplified distribution of the eroded volume over the length of the channel.

In spite of these limitations the conclusions of the importance of groundwater flow for drainage density and stream incision are arguably relatively robust. The model results show that groundwater capture is a somewhat inevitable consequence of coupling groundwater flow, streamflow and erosion equations. Regardless of the exact equations and numerical implementation used, the watertable will always crop out at perennial streams, and the incision of these streams will draw the watertable down. Smaller streams losing their groundwater discharge and eventually falling dry is therefore a logical consequence of differences in incision rate between streams. These conclusions are also supported by previous model studies that found that groundwater flow had a strong effect on erosion (de Vries, 1994; Huang and Niemann, 2006; Barkwith et al., 2015; Zhang et al., 2016) and by observations that found a correlation between permeability, transmissivity, or lithology and drainage density at a number of locations (Carlston, 1963; Luo and Stepinski, 2008; Bloomfield et al., 2011; Luo et al., 2016).

However, one thing that the model does not represent well is the initiation of stream channels. Due to the 2.5D nature of the model the initial topography is represented only in the modelled cross-section, and all streams are effectively parallel. This means that initially, small streams develop in most small depressions. The presence of many small streams divides the water to be discharged over many streams, which each have a very low incision power but are nonetheless considered active streams in the model. In reality, many of these streams would not initiate, because the initial topography would not consist of a set of small depressions that are lined up and connected along an inclined slope. Instead, most of these depressions would be isolated. Therefore the number of active streams at low runtimes should be much smaller than the high number in the model runs reported here (see for example Fig. 12a). In reality, the stream network would develop much more gradually by headward erosion, as shown by natural experiments (Schumm, 1956; Wells et al., 1985; Kashiwaya, 1987; Talling and Sowter, 1999). For the final model results presented in this study the unrealistic initiation of streams is less of a problem, because the stream networks adjusts relatively rapidly in the first few ~~100s to 1000s~~ 10s to 100s of years as stream incision progresses far enough for most of the initial streams to fall dry and for the initial topography to be irrelevant. Therefore for the final model runtime of a ~~100~~ 10,000 years the unrealistic initiation of stream networks does not affect the results. The exception is however, formed by model runs with low transmissivity ($< 10^{-4}$ m^2 s^{-1}) or low ~~intial~~ initial slope ($< 10^{-4}$ m m^{-1}), for which the ability to capture groundwater discharge and the incision power of the streams is too low to escape the initial phase with a dense stream network.

4.2 Groundwater capture

To my knowledge the process of groundwater capture that is illustrated here has not been proposed before. ~~de Vries (1976)~~ De Vries (1976) and de Vries (1994) discussed the opposite process, in which new streams establish themselves when the watertable reaches the land surface following an increase in precipitation and groundwater recharge. Twidale (2004) suggested that stream incision may induce a positive feedback by increasing groundwater flow and runoff to streams that incise faster, but did not provide any further details.

The process of groundwater capture is expected to be important wherever streamflow is dominated either by groundwater discharge or saturation overland flow. In systems where infiltration-excess flow is dominant, which includes most semi-arid and arid regions (Kidron, 2021), groundwater capture could still occur and would determine which streams discharge groundwater and are active perennially, but streams that are detached from the groundwater table would still be able to incise. In addition, groundwater capture may be less important for systems dominated by subsurface stormflow in perched aquifers that are detached from the watertable. The importance of this flow mechanism is however uncertain and under debate (Freeze, 1972; Chifflard et al., 2019).

Note that the difference between the groundwater capture process and the more well studied process of stream capture (Whipple et al., 2017) is that groundwater capture does not require a physical connection between two streams, and may therefore not leave a clear trace in the landscape, as opposed to river capture. The capture of the groundwater discharge of one stream by another results in the first stream falling dry, but the hillslope between these streams remains intact, as can be seen in Fig. 11.

4.3 Comparison with field studies

The model study presented here used climate, hydrology and erosion parameters that were based on the southern Netherlands (de Vries, 1994; Bogaart et al., 2003). The model results match the observed drainage density and rate of incision in the southern Netherlands relatively well. The modelled drainage density after a runtime of 10,000 years is 0.6 streams per km, which is close to the observed average drainage density of approximately 0.5 streams per km (de Vries, 1994, 1995). In addition, the incision of approximately 3 m is also close to the values observed in the southern Netherlands. This means that the model was able to reproduce the current drainage network that likely developed in response to climate and baselevel changes after the end of the Pleistocene (de Vries, 1994; Bogaart et al., 2003).

The negative correlation between transmissivity and drainage density that the model results shows (Figure 13) has been discussed previously in the literature. Carlston (1963) used theoretical considerations to deduce that high transmissivity leads to high rates of baseflow and low rates of direct surface runoff. A compilation of 13 catchments in the eastern USA with similar climate and recharge found a negative linear correlation between baseflow and the square root of drainage density. When assuming that baseflow and transmissivity are correlated linearly this also results in a negative correlation between the square root of drainage density and transmissivity.

560   Figure 19 contains a compilation of quantitative data on transmissivity and drainage density along with the model results presented in this study. The data compilation support a negative correlation between drainage density and transmissivity. Previous work by Bloomfield et al. (2011) found a significant correlation between drainage density and hydraulic conductivity for nine catchments in the Thames basin, UK. In addition, parts of the Oregon Cascades covered by Tertiary and Quaternary rocks showed a remarkable contrast in drainage density and incision that correlates with a difference in hydraulic conductivity
565   and transmissivity (Luo and Stepinski, 2008; Luo et al., 2010).

Although the field data show the same trend as the model results, for low transmissivities ($< 10^{-3}$ m^{2}s^{-1}) the predicted drainage densities in the model sensitivity analysis are much higher than in the Bloomfield et al. (2011), Luo and Stepinski (2008) and Luo et al. (2010) datasets (Figure 19). The reason for the difference is likely the relatively low initial slopes and the relatively high baselevel in the model runs that mimic the low relief in the Southern Netherlands. Low relief and high
570   baselevel limit groundwater capture and lead to high drainage density, as shown by the model sensitivity analysis (Figure 14). In addition, most of the catchments in the Bloomfield et al. (2011) dataset and the Cascades are bedrock catchments with very different erosion parameters compared to the unconsolidated sediments in the southern Netherlands. Note that the values of transmissivity for the Bloomfield et al. (2011), Luo and Stepinski (2008) and Luo et al. (2010) datasets shown in Fig. 19 are relatively uncertain. Transmissivity was estimated from reported hydraulic conductivity values using an estimated aquifer
575   thickness of 100 m. The hydraulic conductivity values in the Bloomfield et al. (2011) dataset are partly based on grey literature and analogies with lithological units elsewhere. The values reported by Luo and Stepinski (2008) and Luo et al. (2010) are based on a method where the watertable is assumed to be at the surface at groundwater divides. This is not likely to be true in all cases, and these values should therefore be considered minimum estimates.
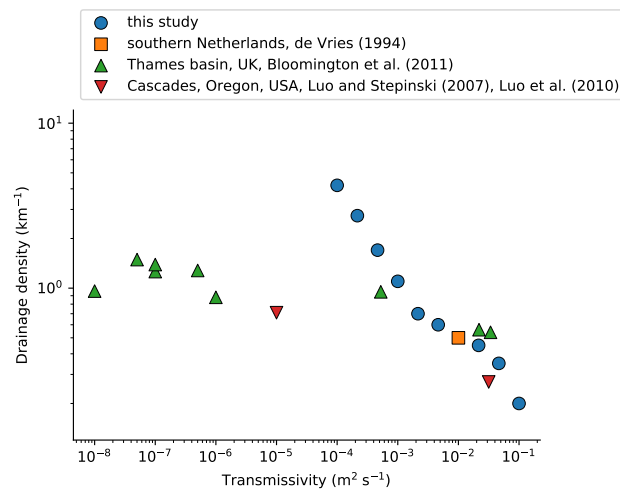
Figure 19. Comparison between the modelled relation between transmissivity and drainage density and field observations (Bloomfield et al., 2011; Luo and Stepinski, 2008; Luo et al., 2010; de Vries, 1994). The reported hydraulic conductivity values by Bloomfield et al. (2011), Luo and Stepinski (2008) and Luo et al. (2010) were converted to transmissivity by multiplication with an estimated aquifer thickness of 100 m. The model results and the field data both show a negative correlation between drainage density and transmissivity. The difference in magnitude are probably related to differences in relief and geology.

4.4   Implications for landscape evolution modelling

580   The strong correlation between drainage density, transmissivity and groundwater flow shown in both the model results and field data means that the inclusion of groundwater flow and a representation of the watertable could strongly improve models of stream network evolution, landscape evolution and water and sediment fluxes over geological ($> \approx 10^4$ a) timescales. The approach shown in this study relies on a partitioning of rainfall in overland flow and groundwater flow, with groundwater flow assumed to be steady-state. The advantage of modelling steady-state, depth-integrated groundwater flow are simplicity and

585   low-computational demands. The exchange between groundwater and surface water was modelled using a seepage algorithm. Similar seepage or drainage algorithms are also able to efficiently couple surface water and groundwater flow in depth-integrated 2D or full 3D models of groundwater flow (Batelaan and De Smedt, 2004) and would therefore be readily available for integration with existing landscape evolution model codes. The assumption of steady-state groundwater flow used in this study is a simplification that omits the effects of transient groundwater discharge. Transient groundwater discharge may be important to

590   include in landscape models, because transient peak groundwater flow rates to streams may have a large effect on erosion. However, three-dimensional models of coupled transient groundwater and surface water flow tend to be computationally demanding and often require parallel computing architectures (Kuffour et al., 2020), which limits the possibility to explore parameter space and model sensitivity. Simplified descriptions of transient groundwater flow similar to the new equation for the integrated discharge and erosion by overland flow events (section 2.6.4 and 2.7.3) could be developed and added to landscape

595   model codes. Such an approach could help constrain the importance of transient groundwater flow for stream incision for different hydrological parameters and different geographic settings.

In addition to being potentially beneficial for models of landscape evolution, a tighter integration of landscape evolution and groundwater models could also improve knowledge of groundwater and surface water systems. The groundwater table is often assumed to follow the topography to some degree and groundwater divides are often assumed to coincide with surface water

600   divides (Liu et al., 2020). However, the validity of this assumption in different geological settings is uncertain. Integrated landscape and groundwater flow models could help quantify the extent to which the watertable can be expected to follow topography and the extent to which surface water divides and groundwater divides are expected to coincide.

5 Conclusions

A new model is presented that couples equations that govern groundwater flow, overland flow, streamflow and erosion and represents humid regions where infiltration-excess overland flow is negligible. The coupling of these equations reveals a strong dependence of drainage density on groundwater flow and transmissivity. The dependence of drainage density on groundwater flow is controlled by a process identified here as groundwater capture, by which faster incising streams draw the watertable below neighbouring streams, which fall dry and lose the ability to incise any further. This process is more efficient when the watertable is relatively flat, which can be either due to low groundwater recharge or high transmissivity, with transmissivity often being the dominant control due to its high variability. Sensitivity analysis show that the importance of transmissivity for drainage density is roughly equal to ~~parameters that control the incision power of stream channels. The importance of transmissivity~~ base level and initial slope and exceeds other hydrological and erosion parameters such as precipitation and hillslope diffusion coefficient. The results _agree with published field data from the Thames Basin, UK, and the Cascades, USA, that show a negative correlation between transmissivity and drainage density. The results_ imply that groundwater and transmissivity may be a dominant control on drainage density in humid regions. Landscape evolution models may need to include groundwater flow and the watertable. At the same time a closer integration of landscape and groundwater data and models may help improve knowledge of the evolution of the earth's surface.

Code availability. The model code presented in this manuscript is named the groundwater flow, overland flow and erosion model, GOEMod, and has been published at Zenodo (Luijendijk, 2021). The code is also available at GitHub (https://github.com/ElcoLuijendijk/goemod). The code is distributed under the GNU General Public License, version 3. The code includes a Jupyter notebook to execute a single model run, which can be used to reproduce Fig. 10, 11 and 12 (https://github.com/ElcoLuijendijk/goemod/blob/master/goemod.ipynb), and a Python script to execute multiple model runs that can be used for model sensitivity analysis, such as presented in Fig. 14 (https://github.com/ElcoLuijendijk/goemod/blob/master/goemod_multiple_runs.py). GOEMod depends on the Python modules Numpy (Harris et al., 2020), Matplotlib (Hunter, 2007), Pandas (McKinney, 2010; Reback et al., 2021) and Scientific colour maps (Crameri, 2021).

Competing interests. The author declares that no competing interests are present

Acknowledgements. I would like to thank J.J. de Vries for sparking my interest in the relation between groundwater systems and landscape evolution.

References

Abrams, D. M., Lobkovsky, A. E., Petroff, A. P., Straub, K. M., McElroy, B., Mohrig, D. C., Kudrolli, A., and Rothman, D. H.: Growth Laws for Channel Networks Incised by Groundwater Flow, Nature Geoscience, 2, 193–196, https://doi.org/10.1038/ngeo432, 2009.

Barkwith, A., Hurst, M. D., Jackson, C. R., Wang, L., Ellis, M. A., and Coulthard, T. J.: Simulating the Influences of Groundwater on Regional Geomorphology Using a Distributed, Dynamic, Landscape Evolution Modelling Platform, Environmental Modelling and Software, 74, 1–20, https://doi.org/10.1016/j.envsoft.2015.09.001, 2015.

Batelaan, O. and De Smedt, F.: SEEPAGE, a New MODFLOW DRAIN Package., Ground water, 42, 576–88, 2004.

Beersma, J., Hakvoort, H., Jilderda, R., Overeem, A., and Versteeg, R.: Neerslagstatistiek En -Reeksen Voor Het Waterbeheer 2019, Tech. rep., Stichting teogepast onderzoek waterbeheer, Amersfoort, 2019.

Bloomfield, J. P., Bricker, S. H., and Newell, A. J.: Some Relationships between Lithology, Basin Form and Hydrology: A Case Study from the Thames Basin, UK, Hydrological Processes, 25, 2518–2530, https://doi.org/10.1002/hyp.8024, 2011.

Bogaart, P. W., Tucker, G. E., and de Vries, J. J.: Channel Network Morphology and Sediment Dynamics under Alternating Periglacial and Temperate Regimes: A Numerical Simulation Study, Geomorphology, 54, 257–277, https://doi.org/10.1016/S0169-555X(02)00360-4, 2003.

Bresciani, E., Goderniaux, P., and Batelaan, O.: Hydrogeological Controls of Water Table-Land Surface Interactions, Geophysical Research Letters, 43, 9653–9661, https://doi.org/10.1002/2016GL070618, 2016.

Brocard, G., Teyssier, C., Dunlap, W. J., Authemayou, C., Simon-Labric, T., Cacao-Chiquín, E. N., Gutiérrez-Orrego, A., and Morán-Ical, S.: Reorganization of a Deeply Incised Drainage: Role of Deformation, Sedimentation and Groundwater Flow, Basin Research, 23, 631–651, https://doi.org/10.1111/j.1365-2117.2011.00510.x, 2011.

Brownlie, W. R.: Compilation of Alluvial Channel Data: Laboratory and Field, California Institute of Technology, WM Keck Laboratory of Hydraulics and and Water Resources, 1981.

Carlston, C. W.: Drainage Density and Streamflow, U.S. Geol. Surv. Prof. Pap. No. 42, pp. 2–C, 8pp, 1963.

Chifflard, P., Blume, T., Maerker, K., Hopp, L., van Meerveld, I., Graef, T., Gronz, O., Hartmann, A., Kohl, B., Martini, E., Reinhardt-Imjela, C., Reiss, M., Rinderer, M., and Achleitner, S.: How Can We Model Subsurface Stormflow at the Catchment Scale If We Cannot Measure It?, Hydrological Processes, 33, 1378–1385, https://doi.org/10.1002/hyp.13407, 2019.

Crameri, F.: Scientific Colour Maps, https://doi.org/10.5281/zenodo.4491293, 2021.

Culling, W. E. H.: Analytical Theory of Erosion, The Journal of Geology, 68, 336–344, 1960.

Culling, W. E. H.: Soil Creep and the Development of Hillside Slopes, The Journal of Geology, 71, 127–161, https://doi.org/10.1086/626891, 1963.

de Vries, J.: Seasonal Expansion and Contraction of Stream Networks in Shallow Groundwater Systems, Journal of Hydrology, 170, 15–26, https://doi.org/10.1016/0022-1694(95)02684-H, 1995.

de Vries, J. J.: The Groundwater Outcrop-Erosion Model; Evolution of the Stream Network in The Netherlands, Journal of Hydrology, 29, 43–50, https://doi.org/10.1016/0022-1694(76)90004-4, 1976.

de Vries, J. J.: Dynamics of the Interface between Streams and Groundwater Systems in Lowland Areas, with Reference to Stream Net Evolution, Journal of Hydrology, 155, 39–56, https://doi.org/10.1016/0022-1694(94)90157-0, 1994.

Dunne, T.: Field Studies of Hillslope Flow Processes, in: Hillslope Hydrology, edited by Kirkby, M., pp. 227–293, John Wiley and sons, Chichester, 1978.

Dunne, T.: Hydrologyy Mechanics, and Geomorphic Implications of Erosion by Subsurface Flow, Special Paper of the Geological Society of America, 252, 1–28, https://doi.org/10.1130/SPE252-p1, 1990.

Dunne, T. and Black, R. D.: An Experimental Investigation of Runoff Production in Permeable Soils, Water Resources Research, 6, 478–490, https://doi.org/10.1029/WR006i002p00478, 1970.

El-husseiny, A.: Improved Packing Model for Functionally Graded Sand-Fines Mixtures — Incorporation of Fines Cohesive Packing Behavior, applied sciences, 10, 23–26, https://doi.org/10.3390/app10020562, 2020.

Forchheimer, P.: Über Die Ergiebigkeit von Brunnen, Anlagen Und Sickerschlitzen, Zeitsch Archit. Ing. Ver., Hannover, 32, 539–563, 1886.

Freeze, R. A.: Role of Subsurface Flow in Generating Surface Runoff 2. Upstream Source Areas, Water Resources Research, 8, 1272–1283, 1972.

Gauckler, P.: Etudes Théoriques et Pratiques Sur l'Ecoulement et Le Mouvement Des Eaux, Comptes Rendues de l'Académie des Sciences, 64, 818–822, 1867.

Gleeson, T., Smith, L., Moosdorf, N., Hartmann, J., Dürr, H. H., Manning, A. H., van Beek, L. P. H., and Jellinek, A. M.: Mapping Permeability over the Surface of the Earth, Geophysical Research Letters, 38, 1–6, https://doi.org/10.1029/2010GL045565, 2011.

Gleeson, T., Moosdorf, N., Hartmann, J., and van Beek, L. P. H.: A Glimpse beneath Earth's Surface: GLobal HYdrogeology MaPS (GLHYMPS) of Permeability and Porosity, Geophysical Research Letters, 41, 1–8, https://doi.org/10.1002/2014GL059856, 2014.

Gleeson, T., Befus, K., Jasechko, S., Luijendijk, E., and Cardenas, M. B.: Global_modern_groundwater_Gleesonetal, figshare Dataset, https://doi.org/10.6084/m9.figshare.1560081.v3, 2016.

Harel, M. A., Mudd, S. M., and Attal, M.: Global Analysis of the Stream Power Law Parameters Based on Worldwide 10Be Denudation Rates, Geomorphology, 268, 184–196, https://doi.org/10.1016/j.geomorph.2016.05.035, 2016.

Harris, C. R., Millman, K. J., van der Walt, S. J., Gommers, R., Virtanen, P., Cournapeau, D., Wieser, E., Taylor, J., Berg, S., Smith, N. J., Kern, R., Picus, M., Hoyer, S., van Kerkwijk, M. H., Brett, M., Haldane, A., del Río, J. F., Wiebe, M., Peterson, P., Gérard-Marchant, P., Sheppard, K., Reddy, T., Weckesser, W., Abbasi, H., Gohlke, C., and Oliphant, T. E.: Array Programming with NumPy, Nature, 585, 357–362, https://doi.org/10.1038/s41586-020-2649-2, 2020.

Howard, A. D.: Badland Morphology and Evolution: Interpretation Using a Simulation Model, Earth Surface Processes and Landforms, 22, 211–227, https://doi.org/10.1002/(SICI)1096-9837(199703)22:3<211::AID-ESP749>3.0.CO;2-E, 1997.

Huang, X. and Niemann, J. D.: Modelling the Potential Impacts of Groundwater Hydrology on Long-Term Drainage Basin Evolution, Earth Surface Processes and Landforms, 31, 1802–1823, https://doi.org/10.1002/esp.1369, 2006.

Hunter, J. D.: Matplotlib: A 2D Graphics Environment, Computing in Science & Engineering, 9, 90–95, https://doi.org/10.1109/MCSE.2007.55, 2007.

Jasechko, S., Perrone, D., Befus, K. M., Bayani Cardenas, M., Ferguson, G., Gleeson, T., Luijendijk, E., McDonnell, J. J., Taylor, R. G., Wada, Y., and Kirchner, J. W.: Global Aquifers Dominated by Fossil Groundwaters but Wells Vulnerable to Modern Contamination, Nature Geoscience, 10, 425–429, https://doi.org/10.1038/ngeo2943, 2017.

Kashiwaya, K.: Theoretical Investigation of the Time Variation of Drainage Density, Earth Surface Processes and Landforms, 12, 39–46, 1987.

Kidron, G. J.: Comparing Overland Flow Processes between Semiarid and Humid Regions: Does Saturation Overland Flow Take Place in Semiarid Regions?, Journal of Hydrology, 593, 125 624, https://doi.org/10.1016/j.jhydrol.2020.125624, 2021.

Kuffour, B. N. O., Engdahl, N. B., Woodward, C. S., Condon, L. E., Kollet, S., and Maxwell, R. M.: Simulating Coupled Surface–Subsurface Flows with ParFlow v3.5.0: Capabilities, Applications, and Ongoing Development of an Open-Source, Massively Parallel, Integrated Hydrologic Model, Geoscientific Model Development, 13, 1373–1397, https://doi.org/10.5194/gmd-13-1373-2020, 2020.

705 Lacey, G.: Stable Channels in Alluvium, Minutes of the Proceedings of the Institution of Civil Engineers, 229, 259–292, https://doi.org/10.1680/imotp.1930.15592, 1930.

Lammers, R. W. and Bledsoe, B. P.: Parsimonious Sediment Transport Equations Based on Bagnold's Stream Power Approach: Stream Power Based Sediment Transport Equations, Earth Surface Processes and Landforms, 43, 242–258, https://doi.org/10.1002/esp.4237, 2018.

Litwin, D. G., Tucker, G. E., Barnhart, K. R., and Harman, C. J.: GroundwaterDupuitPercolator: A Landlab Component for Groundwater Flow, Journal of Open Source Software, 5, 1935, https://doi.org/10.21105/joss.01935, 2020.

710 Liu, Y., Wagener, T., Beck, H. E., and Hartmann, A.: What Is the Hydrologically Effective Area of a Catchment?, Environmental Research Letters, 15, 104 024, https://doi.org/10.1088/1748-9326/aba7e5, 2020.

Luijendijk, E.: GOEMod: Groundwater Flow, Overland Flow and Erosion Model, https://doi.org/10.5281/zenodo.4663728, 2021.

Luijendijk, E. and Gleeson, T.: How Well Can We Predict Permeability in Sedimentary Basins? Deriving and Evaluating Porosity-Permeability Equations for Noncemented Sand and Clay Mixtures, Geofluids, 15, 67–83, https://doi.org/10.1111/gfl.12115, 2015.

715 Luo, W. and Pederson, D. T.: Hydraulic Conductivity of the High Plains Aquifer Re-Evaluated Using Surface Drainage Patterns, Geophysical Research Letters, 39, 1–6, https://doi.org/10.1029/2011GL050200, 2012.

Luo, W. and Stepinski, T.: Identification of Geologic Contrasts from Landscape Dissection Pattern: An Application to the Cascade Range, Oregon, USA, Geomorphology, 99, 90–98, https://doi.org/10.1016/j.geomorph.2007.10.014, 2008.

Luo, W., Grudzinski, B. P., and Pederson, D.: Estimating Hydraulic Conductivity from Drainage Patterns-a Case Study in the Oregon

720 Cascades, Geology, 38, 335–338, https://doi.org/10.1130/G30816.1, 2010.

Luo, W., Jasiewicz, J., Stepinski, T., Wang, J., Xu, C., and Cang, X.: Spatial Association between Dissection Density and Environmental Factors over the Entire Conterminous United States, Geophysical Research Letters, 43, 692–700, https://doi.org/10.1002/2015GL066941, 2016.

Manning, R.: On the Flow of Water in Open Channels and Pipes, Transactions of the Institution of Civil Engineers of Ireland, 20, 161–207,

725 1891.

McKinney, W.: Data Structures for Statistical Computing in Python, in: Proceedings of the 9th Python in Science Conference, edited by van der Walt, S. and Millman, J., pp. 56–61, https://doi.org/10.25080/Majora-92bf1922-00a, 2010.

Moeck, C., Grech-Cumbo, N., Podgorski, J., Bretzler, A., Gurdak, J. J., Berg, M., and Schirmer, M.: A Global-Scale Dataset of Direct Natural Groundwater Recharge Rates: A Review of Variables, Processes and Relationships, Science of The Total Environment, 717,

730 137 042, https://doi.org/10.1016/j.scitotenv.2020.137042, 2020.

Montgomery, D. R. and Dietrich, W. E.: Channel Initiation and the Problem of Landscape Scale, Science, 255, 826 LP – 830, https://doi.org/10.1126/science.255.5046.826, 1992.

Pederson, D. T.: Stream Piracy Revisited: A Groundwater-Sapping Solution, GSA Today, 11, 4–11, 2001.

Perron, J. T., Dietrich, W. E., and Kirchner, J. W.: Controls on the Spacing of First-Order Valleys, Journal of Geophysical Research: Earth

735 Surface, 113, https://doi.org/10.1029/2007JF000977, 2008.

Perron, J. T., Kirchner, J. W., and Dietrich, W. E.: Formation of Evenly Spaced Ridges and Valleys, Nature, 460, 502–505, https://doi.org/10.1038/nature08174, 2009.

Perron, J. T., Richardson, P. W., Ferrier, K. L., and Lapotre, M.: The Root of Branching River Networks, Nature, 492, 100–103, https://doi.org/10.1038/nature11672, 2012.

740 Reback, J., McKinney, W., jbrockmendel, den Bossche, J. V., Augspurger, T., Cloud, P., gfyoung, Hawkins, S., Sinhrks, Roeschke, M., Klein, A., Petersen, T., Tratner, J., She, C., Ayd, W., Naveh, S., Garcia, M., Schendel, J., patrick, Hayden, A., Saxton, D., Jancauskas, V., McMaster, A., Gorelli, M., Battiston, P., Seabold, S., Dong, K., chris-b1, h-vetinari, and Hoyer, S.: Pandas-Dev/Pandas: Pandas 1.2.2, https://doi.org/10.5281/zenodo.4524629, 2021.

Revil, A.: Mechanical Compaction of Sand/Clay Mixtures, Journal of Geophysical Research, 107, 1–11, 745 https://doi.org/10.1029/2001JB000318, 2002.

Richardson, P. W., Perron, J. T., and Schurr, N. D.: Influences of Climate and Life on Hillslope Sediment Transport, Geology, 47, 423–426, https://doi.org/10.1130/G45305.1, 2019.

Schumm, S. A.: Evolution of Draiange Systems and Slopes in Badlands at Perth Amboy, New Jersey, Bulletin of the Geological Society of America, 67, 579–646, 1956.

750 Talling, P. J. and Sowter, M. J.: Drainage Density on Progressively Tilted Surfaces with Different Gradients, Wheeler Ridge, California, Earth Surface Processes and Landforms, 24, 809–824, https://doi.org/10.1002/(SICI)1096-9837(199908)24:9<809::AID-ESP13>3.0.CO;2-R, 1999.

Tucker, G., Lancaster, S., Gasparini, N., and Bras, R.: The Channel-Hillslope Integrated Landscape Development Model (CHILD), in: Landscape Erosion and Evolution Modeling, pp. 349–388, Springer, 2001a.

755 Tucker, G. E. and Bras, R. L.: Hillslope Processes, Drainage Density and Landscape Morphology, Water Resources Research, 34, 2751–2764, https://doi.org/doi:10.1029/98WR01474, 1998.

Tucker, G. E. and Hancock, G.: Modelling Landscape Evolution, Earth Surface Processes and Landforms, 35, 28–50, https://doi.org/10.1002/esp.1952, 2010.

Tucker, G. E., Catani, F., Rinaldo, A., and Bras, R. L.: Statistical Analysis of Drainage Density from Digital Terrain Data, Geomorphology, 760 36, 187–202, https://doi.org/10.1016/S0169-555X(00)00056-8, 2001b.

Twidale, C. R.: River Patterns and Their Meaning, Earth-Science Reviews, 67, 159–218, https://doi.org/10.1016/j.earscirev.2004.03.001, 2004.

van den Berg, J. H.: Prediction of Alluvial Channel Pattern of Perennial Rivers, Geomorphology, 12, 259–279, https://doi.org/10.1016/0169-555X(95)00014-V, 1995.

765 van der Meij, W. M., Temme, A., Lin, H. S., Gerke, H. H., and Sommer, M.: On the Role of Hydrologic Processes in Soil and Landscape Evolution Modeling: Concepts, Complications and Partial Solutions, Earth-Science Reviews, 185, 1088–1106, https://doi.org/10.1016/j.earscirev.2018.09.001, 2018.

Wells, S. G., Dohrenwend, J. C., McFadden, L. D., Turrin, B. D., and Mahrer, K. D.: Late Cenozoic Landscape Evolution on Lava Flow Surfaces of the Cima Volcanic Field, Mojave Desert, California., Geological Society of America Bulletin, 96, 1518–1529, 770 https://doi.org/10.1130/0016-7606(1985)96<1518:LCLEOL>2.0.CO;2, 1985.

Whipple, K. X., Forte, A. M., DiBiase, R. A., Gasparini, N. M., and Ouimet, W. B.: Timescales of Landscape Response to Divide Migration and Drainage Capture: Implications for the Role of Divide Mobility in Landscape Evolution, Journal of Geophysical Research: Earth Surface, 122, 248–273, https://doi.org/10.1002/2016JF003973, 2017.

Zhang, Y., Slingerland, R., and Duffy, C.: Fully-Coupled Hydrologic Processes for Modeling Landscape Evolution, Environmental Modelling 775 and Software, 82, 89–107, https://doi.org/10.1016/j.envsoft.2016.04.014, 2016.